Impact of the physical-chemical properties of poly(lactic acid)-poly (ethylene glycol) polymeric nanoparticles on biodistribution

DOI:
10.1016/j.jconrel.2023.11.043

Document Version
Accepted author manuscript

Published in:
Journal of Controlled Release

Journal of Controlled Release

Impact of the Physical-Chemical Properties of Poly(lactic acid)–Poly(ethylene glycol) Polymeric Nanoparticles on Biodistribution

--Manuscript Draft--

Manuscript Number:	COREL-D-23-01687R1
Article Type:	Research paper
Keywords:	Nanoparticles; PLA-PEG; Critical Quality Attributes; biodistribution; in vitro release; Bioanalytical Assay; SANS; Cryo-TEM; HAXPES; characterisation
Corresponding Author:	Mark Jackman AstraZeneca UK Limited UNITED KINGDOM
First Author:	Mark Jackman
Order of Authors:	Mark Jackman
	Weimin Li
	Aaron Smith
	David Workman
	Kevin Treacher
	Adam Corrigan
	Fadi Abdulrazzaq
	Silvia Sonzini
	Zahid Nazir
	M. Jayne Lawrence
	Najet Mahmoudi
	David Cant
	Jonathan Counsell
	Jonathan Cairns
	Doug Ferguson
	Eva Lenz
	Saif Baquain
	Christine M. Madla
	Sally van Pelt
	Jennifer Moss
	Alison Peter
	Sanyogitta Puri
	Marianne Ashford
	Mariarosa Mazza
Abstract:	Nanoparticle (NP) formulations are inherently polydisperse making their structural characterization complex. It is essential, however, to gain an understanding of the physico-chemical properties that drive performance in vivo. To elucidate these properties, drug-containing poly(lactic acid) (PLA)–poly(ethylene glycol) (PEG) block polymeric NP formulations (or PNPs) were sub-divided into discrete size fractions and analyzed using a combination of advanced techniques, namely cryogenic transmission electron microscopy, small-angle neutron and X-ray scattering, nuclear magnetic

	resonance, and hard-energy X-ray photoelectron spectroscopy. Together, these techniques revealed a uniquely detailed picture of PNP size, surface structure, internal molecular architecture and the preferred site(s) of incorporation of the hydrophobic drug, AZD5991, properties which cannot be accessed via conventional characterization methodologies. PNP size distribution was established important in determining drug loading, with the presence of the smallest PNPs containing significantly less drug than their larger sized counterparts, reducing overall drug loading, while PNP molecular architecture was critical in understanding the nature of in vitro drug release. The effect of PNP size and structure on drug biodistribution was determined by administrating selected PNP size fractions to mice, with the smaller sized NP fractions increasing the total drug-plasma concentration area under the curve and reducing drug concentrations in liver and spleen, due to greater avoidance of the reticuloendothelial system. In contrast, administration of unfractionated PNPs, containing a large population of NPs with extremely low drug load, did not significantly impact the drug's pharmacokinetic behaviour - a significant result for nanomedicine development where a uniform formulation is usually an important driver. We also demonstrate how, in this study, it is not practicable to validate the bioanalytical methodology for drug released in vivo due to the NP formulation properties, a process which is applicable for most small molecule-releasing nanomedicines. In conclusion, this work details a strategy for determining the effect of formulation variability on in vivo performance, thereby informing the translation of PNPs, and other NPs, from the laboratory to the clinic.

Impact of the Physical-Chemical Properties of Poly(lactic acid)–Poly(ethylene glycol) Polymeric Nanoparticles on Biodistribution

Mark J. Jackman,*[a] Weimin Li,[a] Aaron Smith,[b] David Workman,[a] Kevin Treacher,[c] Adam Corrigan,[d] Fadi Abdulrazzaq,[a] Silvia Sonzini,[a] Zahid Nazir,[c] M. Jayne Lawrence,[e] Najet Mahmoudi,[f] David Cant,[g] Jonathan Counsell,[h] Jonathan Cairns,[d] Doug Ferguson,[i] Eva Lenz,[j] Saif Baquain,[a†] Christine M. Madla,[a‡] Sally van Pelt,[k] Jennifer Moss,[l] Alison Peter,[l] Sanyogitta Puri,[a] Marianne Ashford,[m] Mariarosa Mazza*[a]

[a]Advanced Drug Delivery, Pharmaceutical Sciences, R&D, AstraZeneca, Cambridge, UK; [b]DMPK, Oncology R&D, AstraZeneca, Cambridge, UK; [c]New Modalities & Parenteral Development, Pharmaceutical Technology & Development, Operations, AstraZeneca, Macclesfield, UK; [d]Data Sciences and Quantitative Biology, Discovery Sciences, R&D, AstraZeneca, Cambridge, UK, [e]Division of Pharmacy & Optometry and the North West Centre for Advanced Drug Delivery (NoWCADD), School of Health Sciences, University of Manchester, Manchester, UK; [f]ISIS Pulsed Neutron and Muon Source, Rutherford Appleton Laboratory, Chilton, Didcot, UK; [g]National Physical Laboratory, Teddington; [h]Kratos Analytical, Wharfside, Manchester, UK; [d]Data Sciences and Quantitative Biology, Discovery Sciences, R&D, AstraZeneca, UK; [i]Drug Metabolism and Pharmacokinetics, Early Oncology Research and Development,, AstraZeneca, Waltham, Massachusetts, USA; [j]Medicinal Chemistry, Research and Early Development, Oncology R&D, AstraZeneca, Cambridge, UK; [k]Business, Planning & Operations, AstraZeneca, Cambridge, UK; [l]Bioscience, Oncology R&D, AstraZeneca, Cambridge, UK; [m]Advanced Drug Delivery, Pharmaceutical Sciences, R&D, AstraZeneca, Macclesfield, UK.

ABSTRACT: Nanoparticle (NP) formulations are inherently polydisperse making their structural characterization complex. It is essential, however, to gain an understanding of the physico-chemical properties that drive performance *in vivo*. To elucidate these properties, drug-containing poly(lactic acid) (PLA)–poly(ethylene glycol) (PEG) block polymeric NP formulations (or PNPs) were sub-divided into discrete size fractions and analyzed using a combination of advanced techniques, namely cryogenic transmission electron microscopy, small-angle neutron and X-ray scattering, nuclear magnetic resonance, and hard-energy X-ray photoelectron spectroscopy. Together, these techniques revealed a uniquely detailed picture of PNP size, surface structure, internal molecular architecture and the preferred site(s) of incorporation of the hydrophobic drug, AZD5991, properties which cannot be accessed via conventional characterization methodologies. PNP size distribution was established important in determining drug loading, with the presence of the smallest PNPs containing significantly less drug than their larger sized counterparts, reducing overall drug loading, while PNP molecular architecture was critical in understanding the nature of *in vitro* drug release. The effect of PNP size and structure on drug biodistribution was determined by administrating selected PNP size fractions to mice, with the smaller sized NP fractions increasing the total drug-plasma concentration area under the curve and reducing drug concentrations in liver and spleen, due to greater avoidance of the reticuloendothelial system. In contrast, administration of unfractionated PNPs, containing a large population of NPs with extremely low drug load, did not significantly impact the drug's pharmacokinetic behaviour - a significant result for nanomedicine development where a uniform formulation is usually an important driver. We also demonstrate how, in this study, it is not practicable to validate the bioanalytical methodology for drug released *in* vivo due to the NP formulation properties, a process which is applicable for most small molecule-releasing nanomedicines. In conclusion, this work details a strategy for determining the effect of formulation variability on *in vivo* performance, thereby informing the translation of PNPs, and other NPs, from the laboratory to the clinic.

Over the last few decades, vast numbers of novel nanomedicines intended for delivering a range of therapeutic modalities have been described in the scientific literature.[1] Despite this interest, relatively few nanomedicine formulations have progressed to the clinic. To date, only about 50 medical nanomedicine products have been approved by regulatory bodies in various countries, albeit for a variety of indications.[2-4] Significantly, clinical studies have demonstrated that nanoparticles (NPs) can increase drug safety and/or the accumulation of drugs at the tumor site.[5, 6] For example, polymeric NPs (PNPs) based on poly(lactic acid) (PLA)–poly(ethylene glycol) (PEG) block copolymers have been explored both preclinically and clinically and have been shown to improve the therapeutic index of small-mol-

ecule drugs.[7-10] Although NPs, including PNPs, were developed for therapeutic application more than 40 years ago,[11] progressing these nanomedicines past the preclinical proof-of-concept stages and into the clinic requires, amongst other things, suitable large-scale manufacturing technologies and advanced analytical characterization methodologies. The requirement to maintain the batch-to-batch reproducibility of the nanomedicines and to ensure their consistent product performance has frequently resulted in a bottleneck in the nanomedicine development process.[12]

Ensuring reproducible nanomedicine product performance requires identification and control of selected physical-chemical properties of the NPs, properties known in the pharmaceutical industry as critical quality attributes (CQAs), which are controlled through defined product specifications. The CQAs of NPs, including PNPs, which are designed to ensure the reproducible and consistent preclinical performance of the therapeutic pay-load *in vivo*, include their size, polydispersity, shape, surface properties, drug content, drug release profile and drug loading. Due to the inherent complexities of characterizing NPs, troubleshooting unexpected results frequently requires in-depth and scientifically challenging investigations, often delaying the translation of the NPs from preclinical research into clinical development. Nevertheless, understanding the nature of the NPs and, in particular, selecting the right drug for the right target using the right nanomedicine is critical to progressing the product for clinical application.[13]

The U.S. Food and Drug Administration's (FDA's) 2022 guidance document for the development of nanomaterial containing drug products[14] is centered around the NP's size (1–1000 nm) and the criticality of size to the product's performance.[15] Amongst other things, the FDA's CQAs guidance set expectations for the measurement and control of the average particle size and size distribution. Dynamic light scattering (DLS) is the primary methodology for determining the size and polydispersity index (PDI) of a NP formulation.[16] Although a PDI (i.e. the distribution of NP sizes with a formulation) of ≤ 0.2 is commonly deemed as acceptable for a NP formulation,[17] much lower PDIs are achievable for NP formulations.[18] Indeed it is possible to reduce the distribution of a polydisperse NP formulation by size fractionation.[19] Although fractionation generally leads to the loss of product as well as extra product processing, it can provide insights into the nature and population of the NPs comprising the product and presents a systematic approach to developing acceptance criteria for NPs intended for preclinical studies.

NP size, surface poly(ethylene) glycol (PEG) density and the rate of drug release are three key NP CQAs affecting the plasma circulation time and therapeutic index of drug-loaded NPs. It is widely documented that NP biodistribution is significantly dependent on size with the smaller NPs exhibiting longer plasma circulation times compared to the larger NPs which are predominately taken up in the liver and spleen.[20-25] In addition, the presence of a hydrated outer PEG shell also increases plasma circulation time by reducing NP phagocytosis.[26, 27] Bertrand et al. have demonstrated that maximum PNP circulation time can be achieved with a surface density of > 20 PEG chains per 100 nm.[21] The desired release rate of a drug from an NP is dependent on its pharmacokinetic (PK) properties, the intended therapeutic use of the drug and any adverse effects that limit the drug's therapeutic index.[8, 25]

Drug concentration in plasma is a key performance indicator for drug-loaded NPs, but its measurement is challenging due to the high concentration of drug encapsulated in the NP compared with the relatively low concentration of the drug released into the plasma. Even a small percentage of drug released from the NP after sampling can result in a large overestimate of released drug in the plasma. Various methodologies and approaches have been developed to accurately measure the concentration of released drug,[28-31] but designing verification protocols for these methodologies requires a tailored approach because the nature and therapeutic target of each NP formulation are different.

In this work, we produced drug-loaded PLA-PEG block copolymer nanoparticles (AZDNPs) via a nanoemulsion process, using the modified oil-in-water emulsification solvent extraction method described by Hrkach et al.[32] The drug used in the present study was AZD5991, a macrocyclic Mcl-1 specific inhibitor [33-35]. The goal of preparing a nanoparticle formulation of AZD5991 was to modify the drug's pharmacokinetics properties and to increase its plasma circulation time. The study focuses on the physico-chemical characterization of the NPs and the impact of these properties, particularly NP polydispersity on biodistribution. A visual schematic of the work stream and characterization techniques is shown in Figure 1. Using ultracentrifugation, the bulk 110-nm AZDNPs were fractionated into discrete particle size ranges which were characterized in-depth. It was established that the surface PEG density and drug loading and release rate increased with AZDNP size. Additionally, it was established that overall drug loading was limited by the presence of small size fraction PNPs which incorporated very low levels of drug. Doses of three of the size fractions (mean size of 85, 110, and 145 nm) were administered to mice in a PK study which established that smaller sized AZDNPs increased the area under the plasma drug concentration curve (AUC). Administration to mice of the unfractionated AZDNPs (mean size of 110 nm) found that the presence of PNPs with low drug load did not impede reaching proof of concept for *in vivo* preclinical studies. Finally, it was established that validation of the bioanalytical measurements for drug released from AZDNPs *in vivo* can be severely impacted by the presence of substantial free (unencapsulated) drug in the formulation, with scenarios possible where validation to FDA guidelines may be challenging. Overall, the work presented here demonstrates the variability that can exist within an NP formulation, how the nature of this variability can be characterized, and how its impact on *in vivo* performance can be interrogated when developing nanomedicines with the goal of clinical development.

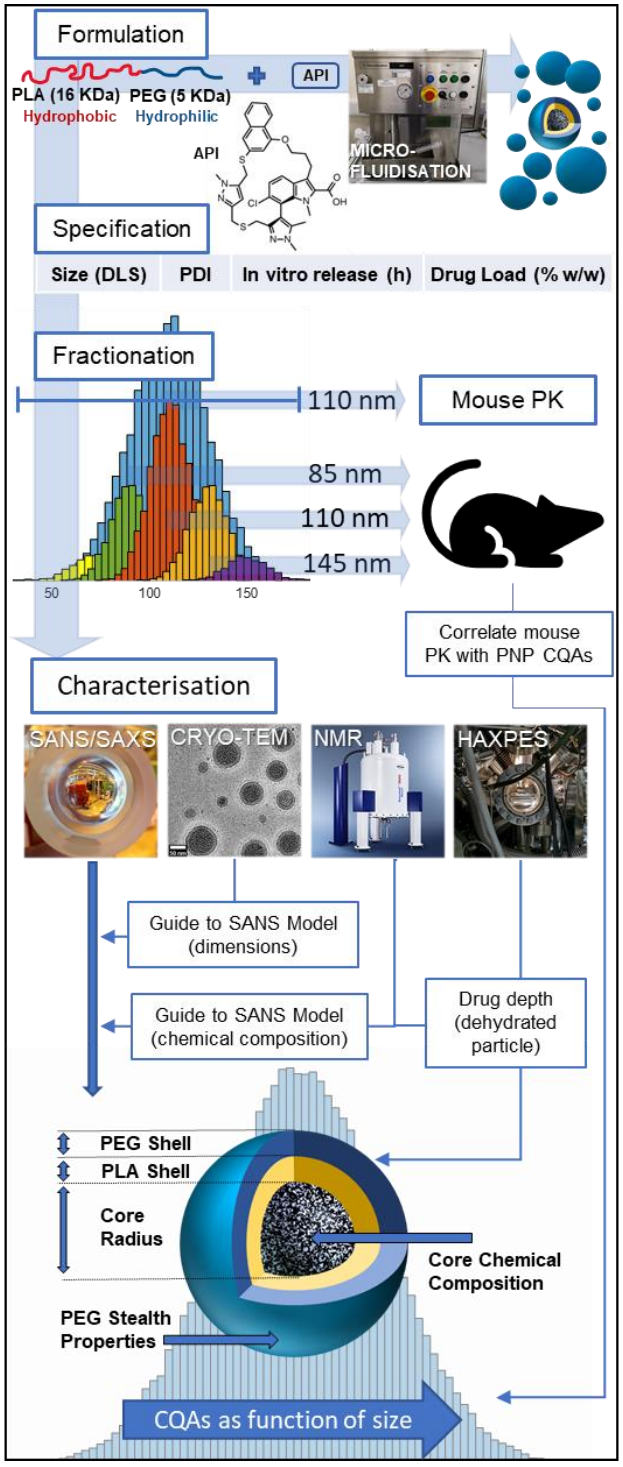

Figure 1. Flow chart of the work performed in this study. Proprietary batches of AZDNPs were prepared by microfluidization and tested to preclinical specifications which included size, polydispersity, drug load, and *in vitro* release ($t_{50\%}$). AZDNPs batches were fractionated into discrete sizes using ultracentrifugation and in-depth characterization performed using NMR, small-angle scattering, cryo-TEM, and HAXPES to determine NP morphology as a function of NP size (as assessed by dynamic light scattering). Three size fractions (85, 110, and 145 nm) and the unfractionated batch of AZDNPs (110 nm) were administered to mice in a pharmacokinetic study to determine how AZDNP size affected biodistribution. Administration of the unfractionated batch (mean size of 110 nm) allowed the effect of formulation polydispersity on biodistribution to be established.

RESULTS AND DISCUSSION

Particle Size Distribution Exhibits an Uneven Drug Load

Two batches of AZDNPs were prepared using either the M-110F and LM20 microfluidizers (which operate on similar principles,[36,37] as described in the Methods), denoted in the text as M-110F AZDNPs and LM20 AZDNPs, respectively. Both batches met internal preclinical specifications and were deemed to be comparable in terms of the physical characteristics described in Table 1.

Table 1. Specification limits and batch data for the (unfractionated) AZDNPs prepared using either the M-110F and LM20 microfluidizers

Test	Specification	M-110F results	LM20 results
Mean particle size by DLS (nm)	50–150	111 ± 2	110 ± 2
DLS polydispersity index (PDI)	< 0.20	0.18	0.13
Drug load (% w/w)	> 10	14.0 ± 0.7	15.6 ± 0.8
Unencapsulated drug (%)	< 5%	4.0 ± 0.3	2.6 ± 0.3
Burst release[a] (%)	< 10%	1.2 ± 0.1	3.7 ± 0.4
In vitro release ($t_{50\%}$)[b] (h)	> 400	660 ± 33	470 ± 20

Note: Error analysis is detailed in the Methods section.
[a] Burst release is a fast release occurring over the first few hours. As stated in the Methods, a two-phase curve was needed to fit the drug release data.
[b] *In vitro* release ($t_{50\%}$) refers to the amount of time for the batch of AZDNPs to release 50% of the encapsulated drug (see Methods for conditions).

Both batches were further separated into discrete size fractions (as determined by dynamic light scattering (DLS)) using ultracentrifugation. The fractions produced from the LM20 instrument had mean diameters of 56, 73, 85, 97, 110, 127, 144, and 157 nm. With the exception of the 144 and 157 nm fractions, which exhibited polydispersity indices (PDIs) of 0.13 and 0.21, respectively, all fractions possessed PDIs of 0.10 or less (**Figure 2**).

Nuclear magnetic resonance (NMR) was used to determine the ratio of the weight of the drug to the combined weight of the drug and polymer, known as the drug to drug plus polymer weight ratio (DDPR) for each NP size fraction. The DDPR was determined by the following equation:

$$DDPR\ (\%\ w/w) = \frac{Weight\ of\ drug\ in\ \_\_\ (mg)}{[Weight\ of\ drug\ in\ formulation\ (mg)] + [weight\ of\ polymer\ in\ formulation\ (mg)]} \times 100$$

The DDPR is analogous to the formulation drug load, but ignores process impurities such as inorganic impurities, inorganics, solvents and residual water within the NPs. The DDPR obtained for all particle size fractions obtained from the LM20 batch are shown in **Figure 2**. Significantly, AZDNPs that were greater than 85 nm in diameter exhibited high drug loads ranging from 20% w/w to 30% w/w, whereas the smaller AZDNP fractions, with diameters of 56 and 75 nm, exhibited low drug loads of 2% w/w and 11% w/w, respectively. The results obtained in the present study fit well with observations made by Huang et al., who reported that, for polylactide-co-glycolide–PEG core shell NPs, drug loading capacity increased with NP size.[38] Troiano et al.[7] and Mares et al.[39] have also reported that NPs of approximately 100 nm size are optimal with respect to drug loading. It was observed that the DDPR of the 110 nm unfractionated batch (PDI = 0.13) was lower at 19% w/w than the 29% w/w obtained for the 110 nm size fraction (PDI = 0.08). Note that the DDPR of the unfractionated batch at 19% w/w was slightly higher than that obtained for the gravimetrically determined drug load, namely 15.6% w/w (**Table 1**), the difference between techniques being a result of the latter measurement taking into account the presence of process impurities. The lower drug loading capacity seen with the unfractionated NPs is undoubtedly a consequence of the presence of the small NPs that contain little, or indeed, no drug.

In Vitro Release Is Dependent on Particle Size

The time taken for 50% of encapsulated drug to be released from the AZDNPs *in vitro* ($t_{50\%}$) was determined for a selection of the AZDNP size fractions prepared from the M-110F and LM20 batches (Supplementary Information S.1). **Figure 2** shows the $t_{50\%}$ curves for a selection of the LM20 AZDNP size fractions as well as the unfractionated batch. A clear, nonlinear trend between AZDNP size (as determined by DLS) and drug release was observed, whereby the smaller 56-nm size AZDNPs released drug significantly faster than the larger sized AZDNPs. In this context, it is significant that the release profile of the 110-nm unfractionated batch ($t_{50\%}$ = 470 hours) was very similar to that determined for the 110-nm size fractionated NPs ($t_{50\%}$ = 500 hours). Similarly, release studies of the fractionated M110F AZDNP batch showed that the $t_{50\%}$ of the unfractionated batch was an average of the $t_{50\%}$ obtained for the different particle size fractions (Supplementary Information S.2). For LM20 AZDNPs, similar levels (< 2%) of unencapsulated ('free') drug were observed in all size fractions except the two smallest size fractions, namely 56 and 73 nm, where levels of 21.8% and 4.0%, of free drug were observed, respectively (**Figure 2**). The differences observed in the percentage of free drug was considered, at least partially, to be a consequence of the ultracentrifugation process, because all the size fractions were expected to yield the same volume of supernatant.

The drug release-time curves (Supplementary Information S.2) could be well fitted using a two-phase exponential. Although the drug release-time curves were dominated by the slow release of drug, thought to be the consequence of diffusion out of the interior of the NP, with the larger NPs exhibiting slower release, all size fractions exhibited the initial, fast burst of drug release (**Figure 2**). While this burst release accounted for less than 5% of total drug release for NPs of a larger size than 85 nm, it increased to nearly 17% when the NPs were 56 nm in size. The fast release of drug observed is thought to be a consequence of drug encapsulated in the hydrated PEG layer on the exterior of the NP.[40] Due to the very low solubility of the drug (< 0.1 mg/mL) in water, the drug is thought to be located in the relatively dehydrated poly(oxyethylene) chain region close to the PEG/PLA boundary. Indeed, it is well established that hydrophobic drugs are well solubilized in concentrated/pure poly(oxyethylene) glycol[41]. As the largest burst effect was observed for the two smallest size fractions, this suggests that a greater proportion of the drug was surface-adsorbed in the smaller AZDNPs (Supplementary Information S.2).

Scattering Techniques and Cryo-TEM Reveal a Core, Two-Shell Nanoparticle Structure

To understand drug release *in vitro* it is necessary first to understand the relationship between the detailed internal architecture of the NPs and the payload they carry. Small-angle neutron and X-ray scattering, techniques sensitive to nuclei and electron density, respectively and cryo-TEM, a technique sensitive to electron density with sub-nanometer resolution, were used in combination to determine, not only the size and shape of the NPs, but also the location of individual components by determining the chemical composition of scattering entities within the NP. **Figure 3a** shows the small-angle neutron scattering (SANS) curves for the various M-110F AZDNP size fractions (prepared using (protiated) co-polymer and containing (protiated) drug) dispersed in D_2O to provide the contrast necessary for the neutron experiments. The corresponding SANS data measured for the unfractionated AZDNPs yielded a relatively featureless scattering curve due to the high polydispersity of the NP formulation (Supplementary Information S.3) which makes it challenging to unambiguously analyze the details of internal structure of the unfractionated formulation.

To analyze the SANS data obtained for the various size fractions studied, a model was needed to describe the internal structure of the AZDNPs. In the present study, the images obtained for the fractionated NPs using cryo-TEM served as a starting point for developing an appropriate model to interpret the SANS data. **Figure 3b** shows representative cryo-TEM images obtained for the 52, 93, and 138 nm size fraction AZDNPs. These images show spherical structures composed of a core surrounded by two-shells. A model to interpret the SANS data was therefore developed by using the information provided by the cryo-TEM images and combining it with a knowledge of the structure of the poly(lactic acid) (PLA)–poly(ethylene glycol) (PEG) block co-polymer. Specifically, the model assumed that the outer of the two shells (seen as the lighter-intensity region in **Figure 3b**) was composed of hydrated PEG chains, a hypothesis subsequently confirmed by proton NMR experiments.[42] As PLA is covalently bonded to PEG, and is more hydrophobic in nature than PEG, the inner of the two shells of the NPs were considered to be (predominantly) comprised of PLA. Finally, the core of the AZDNP was considered to be predominantly composed of drug. Using ImageJ, the cryo-TEM images of the 52, 93 and 138 nm size fractions and the unfractionated (M-110F) batch were analyzed to measure the diameter of the core of the AZDNPs as well as the thickness of

the PLA shell[43,44] (Supplementary Information S.4). The values thus obtained were used as starting points in the model built to analyze the SANS data obtained for the LM20 batch. The value of the neutron SLDs of the various components of the AZDNPs used for modelling the SANS data, are shown in Supplementary Information S.7.

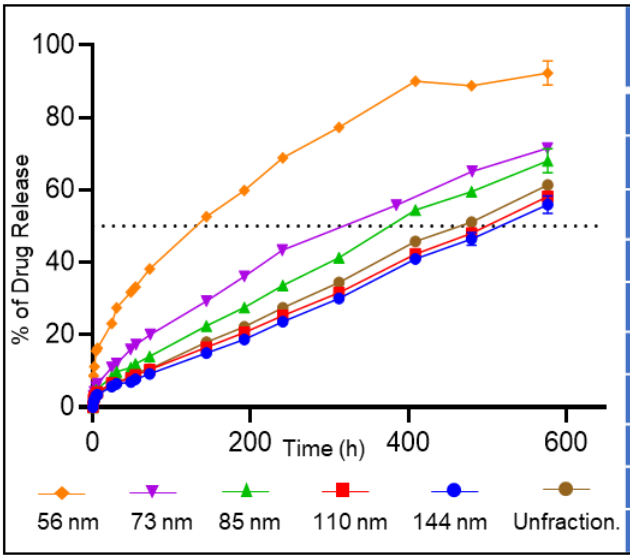

Centrif. force	Size d. (nm)*	PDI	DDPR (% w/w)	Unencap-sulated Drug %	In vitro release $t_{50\%}$ (h)
x 1000 g	DLS	DLS	NMR	UPLC-UV	UPLC-UV
Unfract.	110 ± 2	0.13	19 ± 0	2.6 ± 0.1	470 ± 20
2	157 ± 3	0.21	25 ± 1	1.5 ± 0.1	Not determined
5	144 ± 3	0.13	30 ± 1	1.2 ± 0.1	520 ± 30
10	127 ± 3	0.09	29 ± 1	1.2 ± 0.1	Not determined
20	110 ± 3	0.08	29 ± 1	1.1 ± 0.1	500 ± 20
40	97 ± 2	0.07	25 ± 1	1.4 ± 0.1	Not determined
60	85 ± 1	0.09	20 ± 0	1.9 ± 0.1	375 ± 15
80	73 ± 1	0.10	11 ± 0	4.0 ± 0.2	318 ± 15
120	56 ± 1	0.09	2 ± 0	21.8 ± 1.1	132 ± 15

*Apparent hydrodynamic size

Figure 2. *In vitro* drug release-time curves for the unfractionated batch and a selection of AZDNP size fractions prepared using a LM20 microfluidizer. A dissolution medium of 20% w/v HP-β-CD in 20 mM HEPES at pH 7.4 was used to ensure drug solubility at a final drug concentration of 10 μg/mL (i.e. sink conditions). Experiments were terminated when all size fractions had released at least 50% of their total drug payload. Unencapsulated ('free') drug was removed from the drug release data shown in the Figure as described in Methods section. The Table shows the *in vitro* release data, expressed as the time taken for 50% of encapsulated drug to be released from the AZDNPs ($t_{50\%}$), the apparent hydrodynamic size (determined by dynamic light scattering, marked *), the ratio of the weight of the drug to the combined weight of the drug and polymer (DDPR), and the percentage of unencapsulated drug in the fractionated and unfractionated AZDNPs. Error analysis detailed in Methods section.

In addition to the core, two-shell[45] model, two other models namely an onion[46] model and a core one-shell model[47] were explored to establish which models gave the best fit to the SANS data using physically relevant parameters. (A schematic diagram of these two additional models are given in Supplementary Information S.5. (SASView Models)) The onion model was similar to the core, two-shell model but exploits a gradient of scattering length density (SLD) across the outer hydrated PEG shell. Although two shells were clear from the images produced by the cryo-TEM experiments, for completeness, a core model with one shell was also investigated.[47] Significantly, regardless of the model used to analyse the SANS data, the 144 and 157 nm size fraction AZDNPs could not be modeled because they contained particles that were larger than the size of 300 nm that can be measured by the SANS2d instrument.[48] The radius of gyration (R_g) for each size fraction was determined from the SANS data using the Guinier approximation (Supplementary Information S.6), although once again the SANS data obtained for the 144 and 157 nm size fractions could not be fitted satisfactorily using this methodology. Overall, the best fit to the SANS data was obtained with the onion model (**Figure 3c**) while the poorest fit was obtained with the core one-shell model, although in this latter case satisfactory fits to the data were obtained using this model for the 56 and 73 nm size fractions. The parameters used to obtain the best fit to the SANS data with the onion model are given in Supplementary Information S.5.

Interestingly, because the neutron SLD of PLA is very similar to that of the drug (1.83×10^{-6} versus 1.87×10^{-6} Å^{-2}, respectively), and assuming that only drug and PLA were present, it was not anticipated that SANS measurements made on AZDNs (prepared using protiated co-polymer and containing protiated drug) dispersed in D_2O could be used to determine the ratio of drug to polymer in either the inner shell or core. A similar situation was also anticipated when modelling the X-ray scattering, where the X-ray SLD of PLA (11.7×10^{-6} Å^{-2}), was very similar to that of the drug (11.9×10^{-6} Å^{-2}). Fortuitously, however, despite the use of only one neutron contrast (i.e. protiated AZDNPs in D_2O) differentiation between the composition of the inner shell, proposed to be composed of PLA, and the core was possible, thereby giving insight into the internal structure of the AZDNPs as discussed in more detail under the section, "Drug Core Volume and Porosity Increases with Particle Size."

It is possible to probe the internal structure of the AZDNPs in more depth using SANS measurements exploiting multiple contrast variation, and then by simultaneously modelling the data obtained for the various contrasts. Here, the 97 nm AZDNP size fraction was selected for study using SANS in combination with contrast variation – in total, four neu-

tron contrasts were investigated, namely AZDNPs dispersed in D_2O (1), in H_2O (2), in 34 vol% D_2O in H_2O (3), and in 56 vol% D_2O in H_2O (4). The 34 vol% D_2O contrast was selected because its neutron SLD matches that of PLA and the drug used in the present study, and thereby allows the study of the hydrated PEG shell. A fifth contrast, which could be co-refined with the SANS data, was obtained by performing a small-angle X-ray scattering (SAXS) experiment on AZDNPs dispersed in H_2O. **Figure 3d** shows the resulting scattering curves and the best fit to the scattering data that was obtained by simultaneously fitting the five data sets.[49] The parameters used to obtain the best fit to this experimental data are given in Supplementary Information S.5.

Significantly, the model used to fit the five scattering data sets agreed well with the model used to fit the single contrast data (i.e. protiated AZDNP and drug dispersed in D_2O), thereby giving confidence in the value of the parameters used to obtain the best fit to the single contrast data. The values of the thickness of the outer hydrated PEG shell, the thickness of the inner PLA shell, and the core diameter of the core of the AZDNP fractions thus determined were plotted against the size of the AZDNPs obtained from DLS (**Figure 3e)**. As can be seen, an approximately linear relationship was obtained between both the PLA shell thickness and core diameter with AZDNP size. It is noteworthy that a similar relationship between PLA shell thickness and core diameter with particle size was determined using the cryo-TEM data (Supplementary Information S.4). No such relationship was observed between the thickness of the outer hydrated PEG shell and the size of the AZDNPs in that shell thickness was invariant for the smaller sized AZDNPs and increased in size for the larger AZDNPs. One possible explanation for this observation is that the PEG chains underwent a conformation change upon increasing PEG density for the larger AZDNP from a mushroom to a brush confirmation.[50] To test this hypothesis, in the present study, the density of PEG chains present on the AZDNP surface was estimated using the methodology of Bertrand et al.[21] Plotting the density of the PEG chains against AZDNP size resulted in a linear relationship (Supplementary Information S.9), supporting the hypothesis that the larger size fraction AZDNPs exhibited a higher PEG packing density, confirming that the PEG chains undergo a conformational change with increasing ADNP size, possibly from mushroom to brush conformations. In addition, the higher PEG packing density in the larger size AZDNPs explains why the outer PEG shell was more visible in the cryo-TEM images of these AZDNPs (**Figure 3biii**). Furthermore, the higher density of PEG molecules in the larger AZNPs will also have an impact on hydrophilic PEG chain solvation, resulting in exclusion of water at the PLA/PEG interface and a greater hydration gradient across the shell region. Indeed, all AZDNP size fractions adhered to the > 20 PEG/100 nm^2 criterion identified by Bertrand et al.[21] for maximizing NP circulation in mice.

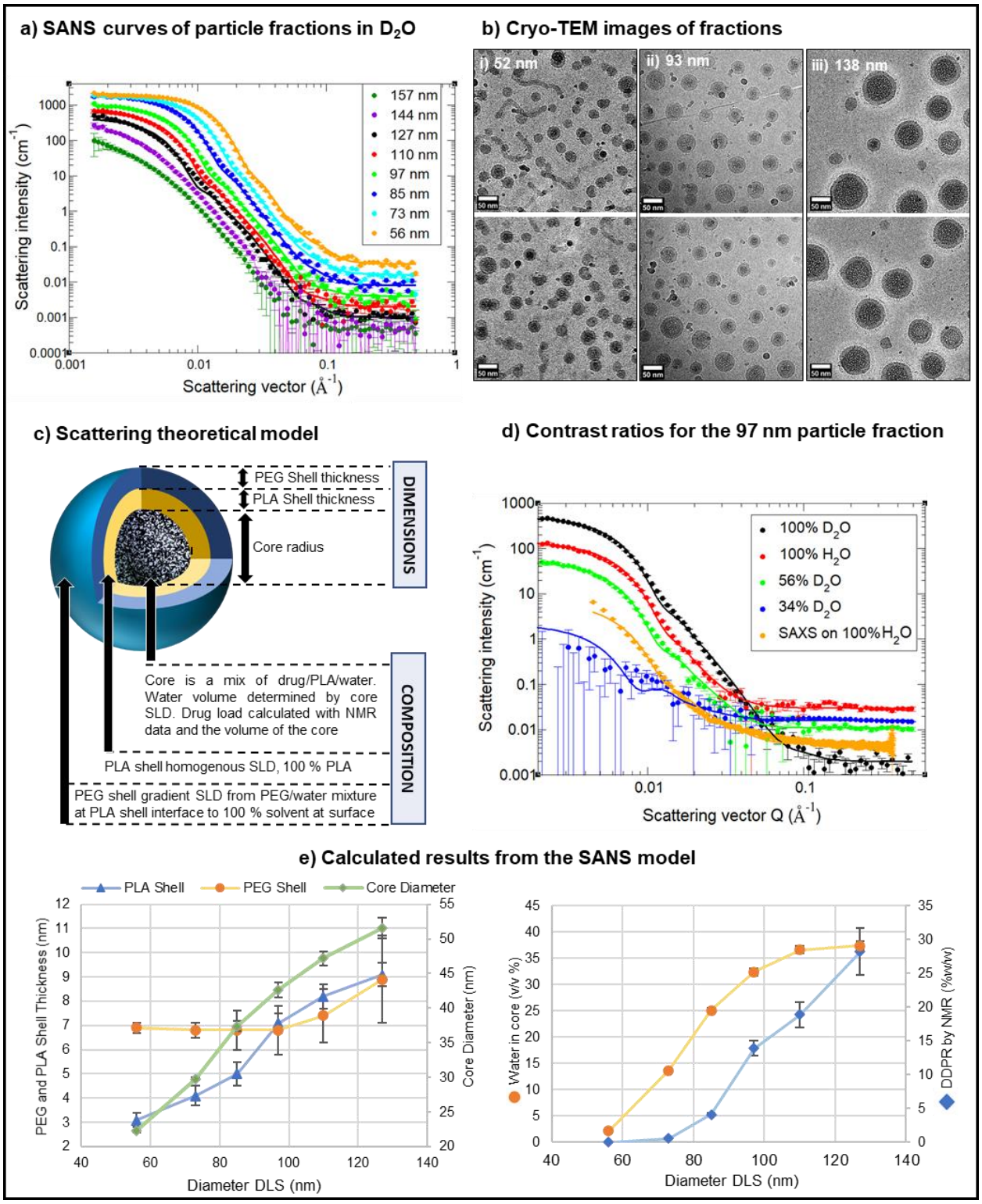

Figure 3. (a) Neutron scattering curves (points) obtained for AZDNPs preparing using a LM20 microfluidizer after fractionation and dialysis in D_2O along with the best fit to the data (solid line) obtained using the onion model (Figure 3c). For ease of visualization offsets (multipliers) were applied to all scattering curves with the exception of that obtained for the 110 nm size fraction; (b) Representative cryo-TEM images of AZDNPs (i) 52 nm, (ii), 93 nm and (iii) 138 nm size fractions prepared using a M-110F microfluidizer, which were used as a starting point for modelling the SANS data; (c) The model proposed from the cryo-TEM and scattering studies; (d) Scattering curves (points) obtained for the five contrasts measured for the LM20 97 nm size fraction AZDNPs (the SAXS data was offset by a multiplier of 5) along with the best fit to the data (solid line) obtained using the model in Figure 3c; (e) Summary of best fit parameters obtained for the size fractions analyzed by SANS (simultaneous fitting of five contrasts for the 97 nm size fraction, and a single contrast for all other size fractions); NMR DDPR included for reference. Complete set of best fit parameters is given in Supplementary Information S.8. Error analysis is detailed in Methods section.

Drug Core Volume and Porosity Increases with Nanoparticle Size

Owing to the similarity of the neutron SLD for the protiated drug and the PLA region of the block copolymer, it had not been expected that the SANS measurement would be able to differentiate between core and the inner PLA shell if only drug and PLA polymer were present in these regions. When the scattering data was modeled for the multi-contrast data for the 97 nm size fraction using with the onion model, the optimal SLD determined for the core using the 100% D_2O was 2.70×10^{-6} Å^{-2} higher than the SLD of either the drug (1.83×10^{-6} Å^{-2}) or the PLA (1.87×10^{-6} Å^{-2}). It was only possible to obtain a SLD of 2.70×10^{-6} Å^{-2} by assuming that some D_2O was also present in the core.

Modelling the single contrast SANS data obtained for all the other NP size fractions studied also yielded a value for the SLD of the core that was higher than that of either PLA and/or the drug. Assuming again that water (D_2O) was present in this region enabled the volume fraction of water in the core to be determined as a function of the AZDNP size fraction (**Figure 3e)**. The volume fraction of water (D_2O) in the core calculated for the 127 nm size fraction AZDNPs was surprisingly large, at ~35 vol%, while this value decreased to virtually 0 for the 52 nm size fraction AZDNPs. The variation of the DDPR as a function of AZDNP size fraction is also plotted in **Figure 3e** and can be seen to broadly follow the same trend as the variation in the volume fraction of water present in the core with AZDNP size fraction. The small size fraction AZDNPs were observed to contain little drug and a relatively low level of water, suggesting that the core is predominantly composed of hydrophobic PLA. However, as the size fraction of the AZDNPs increased, the water content of the core increased as does the DDPR of the NPs. The presence of water in the core was surprising because of the low affinity of the hydrophobic drug for water. It is therefore proposed that high percentage of water in the core could be a consequence of the phase separation of drug and PLA resulting in a porous core, with the pore being filled with water. This hypothesis is supported by the approximately linear relationship observed between the radius of gyration (R_g) and the apparent hydrodynamic radius (R_H), which suggests an increasing porosity[51] with an increase in AZDNP size and supports the observation of an increased water content in the core with increasing AZDNP size (Supplementary Information S.10). A porous core would result in regions of low electron density explaining the white flecks seen in the core of the cryo-TEM images.

Despite the understanding gained as to the detailed internal structure of AZDNPs (summarized in **Figure 3c**) from the combination of cryo-TEM and scattering techniques, obtaining an understanding of the effect of molecular architecture on drug release was more complicated due to the existence of several competing factors. Assuming the slow phase of drug release was due to the release of drug from the core of the NPs, an increase in NP diameter would be expected to increase the diffusion pathlength of the drug leading to a reduced release rate. Opposing this is, as suggested by the cryo-TEM and scattering data, the core becomes more hydrated and porous with an increase in size. As a consequence of the presence of pores, an increase in drug release rate might be anticipated,[52,53] partially counteracting the effect of NP size on drug release. Consideration of these two effects, and noticeably the correlation observed between NPs size and the slow phase of drug release (**Figure 2**) leads to the conclusion that diffusion pathlength dominates the slow release rate.

Orthogonal HAXPES Data Yields Similar Drug Depth to SANS

Photoelectron spectroscopy is a surface-sensitive technique that can be used to probe the top 10 nm of a surface with a conventional aluminum anode. Using a silver anode with higher photoelectron energies, we were able to probe approximately 20 nm into the NP. HAXPES was performed to probe the polymer shell thickness (i.e. the inner PLA shell and the outer PEG shell) within the dehydrated 93-nm AZDNPs (prepared on the M-110F microfluidizer), during which it was important to be aware of size and potential morphology changes when carrying out the analysis. Thickness measurements of the polymer shell around the drug within the AZDNPs were carried out with numerical modeling similar to that utilized by Shard[52-54] and others.[55, 56] For this work, Ag Lα HAXPES also had the advantage over standard X-ray photoelectron spectroscopy (XPS)–based X-ray sources that it could access atomic core levels that are beyond the reach of traditional Al Kα (e.g., the S 1s orbital, as shown in Supplementary Information S.11). In this case, numerical modeling of the HAXPES data was performed using drug loads determined from the NMR data, and an assumed particle diameter based on observed shrinkage of similar particles under high-vacuum conditions. Significantly, when the silver anode was used, the AZDNPs remained stable for several hours under the beam, but using the conventional aluminum source resulted in almost instant beam damage.

Figure 4 shows the selected core-level photoelectron spectra of the 93 nm size fraction AZDNPs. The assignments, binding energies, peak widths, and stoichiometries obtained from the 93 nm size fraction AZDNPs are detailed in Supplementary Information S.11. The polymer shell thickness measured by this method was 4.8 ± 1.0 nm for the 93-nm size fraction AZDNPs. This XPS measurement appears to be smaller than expected; however, any shrinkage of the shell material during sample preparation, dehydration, and introduction to vacuum would reduce the shell thickness (Supplementary Information S.11). In addition to this, due to the exponential attenuation of electron signal passing through an overlayer, thickness calculations performed using photoemission data will always provide a surface-weighted estimate of the average position of a buried material. With these factors in mind, the estimated polymer shell thickness for the 93-nm AZDNP size fraction by XPS (4.8 nm) and SANS (estimated at 7.7 nm) can be considered to give reasonably good agreement, especially considering that the AZDNPs were in different states (i.e., dry in vacuum for XPS, as opposed to in solution for SANS) during measurement. (Note: The M-110F AZDNPs were not measured by SANS, and an estimate was made from the LM20 data and assumptions regarding PEG dehydration [Supplementary Information S.11])

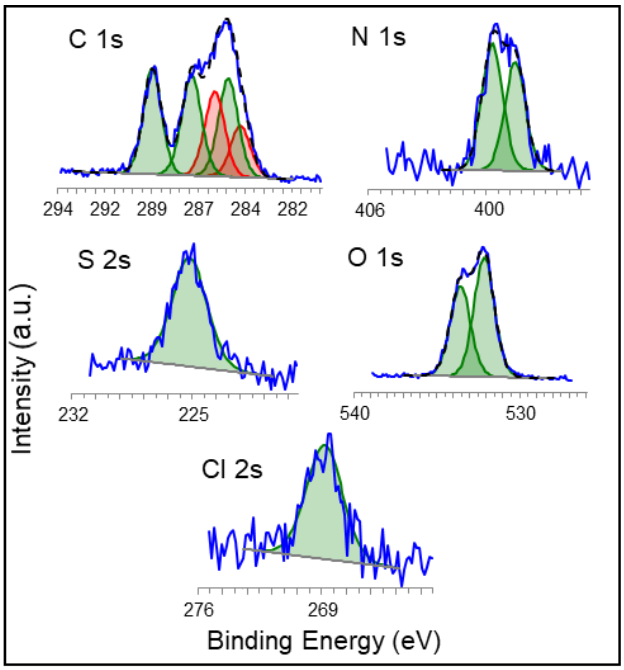

Figure 4. Photoelectron spectra of the 93 nm size fraction AZDNP. Binding energy, assignments, and homogeneous-equivalent atomic concentrations are shown in Supplementary Information S.11.

A Population of Nanoparticles with No Drug Core Lowers the Formulation Drug Load

When the cryo-TEM micrographs obtained for the 52 nm size fractions (**Figure 3bi**) were examined, in addition to many core, two-shell AZDNPs being observed, a number of NPs without any obvious (drug) core were seen, as well as a number of 'snake-like' structures. Interestingly, these 'snake-like' structures were not seen in the cryo-TEMs obtained for the 93 and 138 nm size fractions AZDNPs (**Figures 3 bii** and **biii**, respectively), although some NPs without a drug core were clear in both the 93 and 138 nm size fractions. As a consequence of the presence of the 'snake-like' NPs, the smaller 52 nm size fraction, not surprisingly exhibited a lower drug loading when compared to the other two size fractions where no 'snake-like' NPs were observable (**Figure 2**). Furthermore, the mixed population of NPs with and without drug cores seen in each of the cryo-TEMs of three size fractions, explains why the value of the PLA shell thickness and core radius determined using SANS, averaged over the whole ensemble of NPs and analysed with the onion model were respectively, higher and lower than the corresponding values obtained from the cryo-TEM images, where small numbers of NPs were measured. It should be noted that the cryo-TEM study was aimed primarily at identifying particle morphologies and was not intended for providing statistically significant imaging data. Indeed, in the present study insufficient NP images were taken to generate statistically relevant data. To explore whether these structures are NPs with a low drug-loading, a simple core, one-shell model was used to fit the SANS data obtained for the 56 and 73 nm size fractions (parameters used to obtain the best fit to the SANS data for this and the core, two-shell model are compared in Supplementary Information S.12). It is considered that any drug present in the smallest size fractions AZDNPs would be located in the hydrated PEG layer or at boundary between the PLA-PEG boundaries, and as a consequence the smaller size fraction NPs exhibit a much faster drug release. By way of contrast, in the larger size fractions AZDNPs, most of the drug is thought to reside in the NP core, in which case the inner PLA shell is thought to act as a barrier to the release of drug.

The cryo-TEM image of unfractionated (M-110F) AZDNPs at 75,000 times magnification is shown in Supplementary Information S.13 (Figure S13). As with the cryo-TEM image obtained for the 52 nm size fraction, different types of NPs are observed, with an abundance of snake-like NPs and NPs without a drug core. This observation is likely to be the reason for the large difference between the DDPR obtained for the 110 nm size fraction AZDNPs and the unfractionated 110 nm batch (namely 19% as opposed to 29% w/w, respectively). Of note are the relatively comparable PDIs of 0.13 and 0.08 measured for the unfractionated and fractioned AZDNPs, respectively. The impact of the presence of 'low' drug loaded NPs on the measured plasma circulation time of drug in mice, as well as the effect of AZDNP size on biodistribution, are discussed in the section "Effect of NP Size on Plasma AUC and Liver and Spleen Concentrations."

Validation of Bioanalytical Methods Is Sensitive to the Formulation CQAs: Free (Unencapsulated) Drug Levels and *In Vitro* Release

When progressing to the clinic, it is an FDA requirement to validate the bioanalytical methodology. Validating the measurement of the total concentration of drug in plasma or tissue is a relatively simple measurement, similar to traditional small-molecule bioanalysis, using organic solvent to crash proteins, rupture NPs, and solubilize the drug. However, validating the methodology for measuring the drug that is released from the NPs in the plasma or tissue and is therefore available to bind with biological target(s) is extremely challenging and, depending on the formulation and the dosing regimen, it may not be possible to validate to the FDA requirements of demonstrating errors no greater than 15 %. Due to these challenges, it was decided to not attempt a validation of the methodology and therefore not to quantify the released measurement. Here, we explain why. To validate the method, blood is spiked with known concentration of compound and the NP formulation to create a bio-relevant sample and is then taken through the sample preparation process. Any change in the level of free drug during the preparation of the analytical sample, would indicate the sample preparation process induced drug release from the NPs, and would therefore lead to an overestimation of released drug concentration when analyzing a bioanalytical samples. As some NPs formulations, including these AZDNPs, tend to contain substantial unencapsulated drug, it can be difficult to determine, with sufficient accuracy whether drug has been released in the sample preparation process. This is because when spiking the formulation into the blood to determine accuracy and precision, the unencapsulated drug in the formulation can act as a substantial background within the biological matrix, when looking to measure small changes in unencapsulated drug induced by the sample preparation process. This fact is well demonstrated using a statistical model to investigate the

feasibility of the bioanalytical validation (**Figure 5** and Supplementary Information S.14) and is outlined below. The bioanalytical methodology required for the present study was particularly challenging due to the low concentration of drug released in the plasma relative to the amount still retained (encapsulated) in the NP. Indeed, as evidenced in **Figure 5a** by modelling the PK data, the ratio of drug released from the NP compared to that retained (encapsulated) in the NP is greater than 1:1000, meaning that in blood only 0.1% of the drug is released. Consequently, leakage of only 0.1% of NP encapsulated drug after *in vivo* sampling (either during storage of the sample or due to leakage during preparation of the analytical sample) translates to a 100% error in the measured 'released' drug concentration (**Figure 5b**). Ideally, there would be no free drug in the NP formulation, so that when the blood was spiked with the formulation and taken through the sample preparation process for validation, any measured 'released' drug would indicate a problem with the sample preparation. Unfortunately, the relatively high level of free drug in the AZDNP formulation (~1.9% in the 85 nm size fraction of AZDNPs **(Table 1)**) make it extremely challenging to accurately quantify the degree of drug release induced by the sample preparation process e.g., an increase from 1.9% to 2.0% would be an increase of 0.1%, which, as stated above, would be the equivalent of a 100% overestimate when measuring the amount of drug released *in vivo*. In this respect it is of relevance that FDA guidelines specify a limit of 15% error for bioanalytical analysis.[57] This FDA requirement is exacerbated by the inherent variability in any analytical method (the relative standard deviation [RSD] of six injections of 500 nM drug standard into the LCMS was 10%) (**Figure 5c, 5d**). As the percent increase of free (unencapsulated) drug is smaller than the RSD of the analytical method, many replicates are required to achieve an appropriate level of statistical power. Statistical analysis shows that, to determine whether any drug release has occurred during sample preparation, 20 sample replicates are required to obtain 80% power and to determine whether the method is suitable to detect at least 100% error (**Figure 5e, 5f and Supplementary Information S.14.**). This assessment of error accounts only for sample injection into the LCMS, and not sample preparation, freeze/thaw cycles, or sample stability, which may yield further release of drug and generate further error. The rate of drug release from the NPs also impacts the ability to validate or accurately measure the drug release in the blood. For example, if the ratio of released:encapsulated drug is 1:1000 (as stated above), and the time taken for 50% of encapsulated drug to be released from the NPs ($t_{50\%}$) is 24 hours, after sampling the blood, the scientist has only two minutes to freeze the sample before 0.1 % has been released, which is the equivalent to a 100 % error. There are fundamental barriers to making these measurements in cases where you are unable to generate suitable bio-relevant standards and QCs for validation purposes and these principles are applicable to most drug-releasing nanomedicines designed for the delivery of small molecule drugs. An assessment of the potential for successful validation can be made based on the in vitro release rate, the PK model, and the amount of free drug in the formulation, the latter being the only attribute that the pharmaceutical scientist can control

Effect of NP Size on Plasma AUC and Liver and Spleen Concentrations

To determine the plasma and organ concentrations of drug after administration of AZDNPs as a function of their NP size, female severe combined immune deficient (SCID) mice (n = 6 per NP size fraction) were injected intravenously with a single dose of NP size. Specifically, small (85 nm), medium (110 nm), large (145 nm) size fractions were studied along with unfractionated (110 nm) AZDNP at a concentration of 10 mg/kg, a dose high enough to ensure that drug concentration could be measured accurately over the period of the study. Note here that the total amount of drug measured includes drug both released and still retained (encapsulated) within the AZDNP. The released drug accounts for both the drug that is free in plasma and the drug that is bound to plasma proteins. Live bleeds were performed at 5 minutes and at 0.5, 4, 24, 48, and 72 hours, and organs were harvested at 24 and 144 hours.

Figure 6a shows the concentration of drug in tissues 24 and 144 hours after injection. At 24 hours, the liver concentration of drug for the 145 nm size fraction AZDNPs was 33% higher than for the 110 nm size fraction AZDNPs and 85% higher than for the 85 nm size fraction AZDNPs. At 24 hours, spleen concentrations of drug for the 145 nm size fraction AZDNPs were ~115% higher than for the 110 nm size fraction AZDNPs and ~275% higher than for the 85 nm size fraction AZDNPs. The larger uptake in the organs of the reticuloendothelial system (i.e. liver and spleen) for the larger AZDNPs resulted in lower concentrations in plasma as evidenced by the value of the area under the plasma-time curve, or the AUC, obtained for the various size fractions (**Figures 6b and 6c**), namely the 145 nm size fraction AZDNPs exhibited an AUC ~ 20% and 40% lower than that obtained with the 110 nm and 85 nm size fraction AZDNPs, respectively. This observation may be, at least partially, accounted for by a number of factors. For example, the liver sinusoids have a diameter of 100–150 nm, which will allow the smaller AZDNPs to pass through prior to subsequent hepatocyte exposure.[58] Moreover, liver sinusoidal endothelial cells lining the capillaries carry high-affinity endocytosis receptors which efficiently mediate the uptake of waste substances and avidly pinocytose colloidal particles of less than 200 nm. Also, liver-specialized macrophages (Kupffer cells) have been found to be primarily responsible for the uptake of particles of greater than 200 nm.[59] Lammers et al.[60] and Ouyang et al.[61] have postulated that dosing a trillion NPs to mice leads to overwhelming Kupffer cell uptake and to nonlinearly decreased liver clearance, prolonging NP circulation and increasing NP tumor delivery. In our study, the 145 nm size fraction AZDNP dose was approximately 0.5 trillion NPs, which may account for an efficient liver uptake of the 145 nm NPs by Kupffer cells. The plasma clearance of the drug for the 85 nm size fraction AZDNPs was fairly comparable to that of the 145 nm size fraction AZDNPs, which is interesting when considering that the $t_{50\%}$ was approximately 27% greater for the smaller sized AZDNPs. Furthermore, the 85 nm size fraction AZDNP dose consisted of 3.5 trillion NPs, which could lead to liver saturation and a higher plasma AUC. As shown in **Figure 6c**, when the mass balance was determined (based on limited organ analysis), there was more drug in the body at 24 and 144 hours for the

145 nm size fraction AZDNPs than for the 85 nm size fraction AZDNPs, yet the plasma AUC was ~ 40% lower, suggesting that the smaller AZDNPs were more favorable as slow-release formulations aimed at maximizing plasma drug concentration. Based on the results obtained in the present study, there would be no benefit in reducing the size of the AZDNPs to less than 85 nm, because of the corresponding large reduction in DDPR observed (**Figure 2**). Surprisingly, the 110 nm size fraction AZDNP was present in elevated concentrations in the ovaries and adrenals compared with the 145 and 85 nm size fraction AZDNPs, the reason for which is unclear. The accumulation of PNPs in adrenals and ovaries has already been reported[62-64] and highlights the importance of accounting for sex differences in preclinical screening.[65]

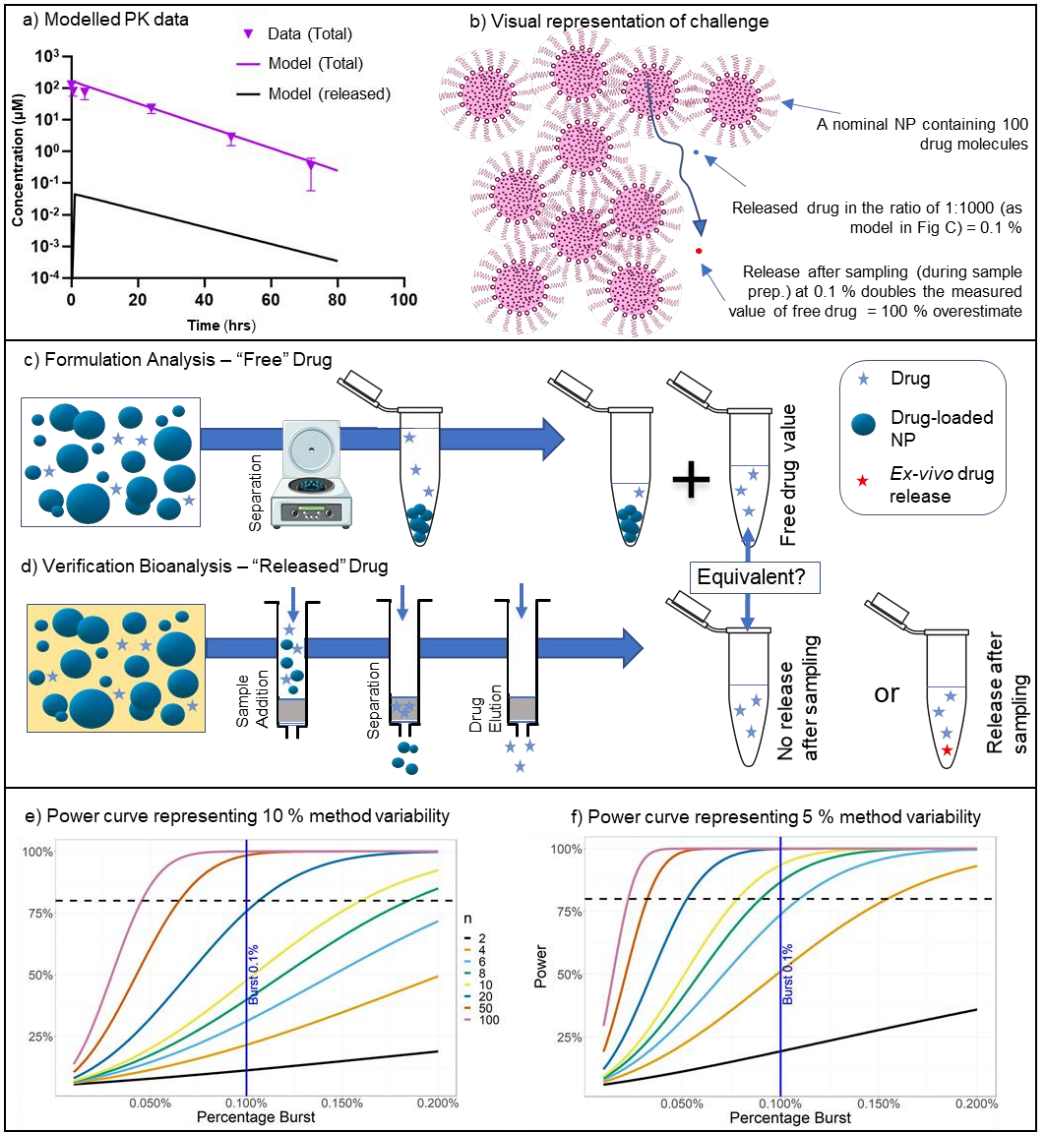

Figure 5. (a) Modeled data based on measured total drug and released drug based on the *in vitro* release $t_{50\%}$ (model developed by Patterson et al.[66]), which estimates a >1:1000 ratio between released and still retained (encapsulated) drug (displayed data and model are for unfractionated AZDNP). (b) Visual representation of how a small amount of drug release in the sampling process/freeze/thaw/sample preparation can significantly influence the measured data. (c) Process for measuring free (unencapsulated) drug in the formulation (described in Methods section). (d) Process for measuring any drug released from the pharmacokinetic (PK) samples during solid-phase extraction (described in Methods section). To verify the sample preparation procedure in the PK samples, the formulation must be spiked into the plasma and the free (unencapsulated) drug recovered. An accurate comparison of the methods is required, with the requirements the methods should yield almost identical results. Method verification difficulties are exacerbated by high levels of free drug in the formulation (~1.9%) used to spike biological media. Detecting this small level of sample leakage (0.1%) in the sample preparation stage needs to be detected with a background of free drug (1.9%) present in the formulation. Power curves were calculated to determine whether it is possible to determine the difference between such small values (0.1%) with method variability of 10% and 5% (e, f). The number of replicates required to reach 80% power with a 10% RSD of injection is too large to be practicably feasible and will still only provide a level of sensitivity able to detect an error of 100% (b). This is in contrast to FDA guidelines that specify a limit of 15% error for bioanalytical analysis.[57] A more detailed analysis is provided in Supplementary Information S.14.

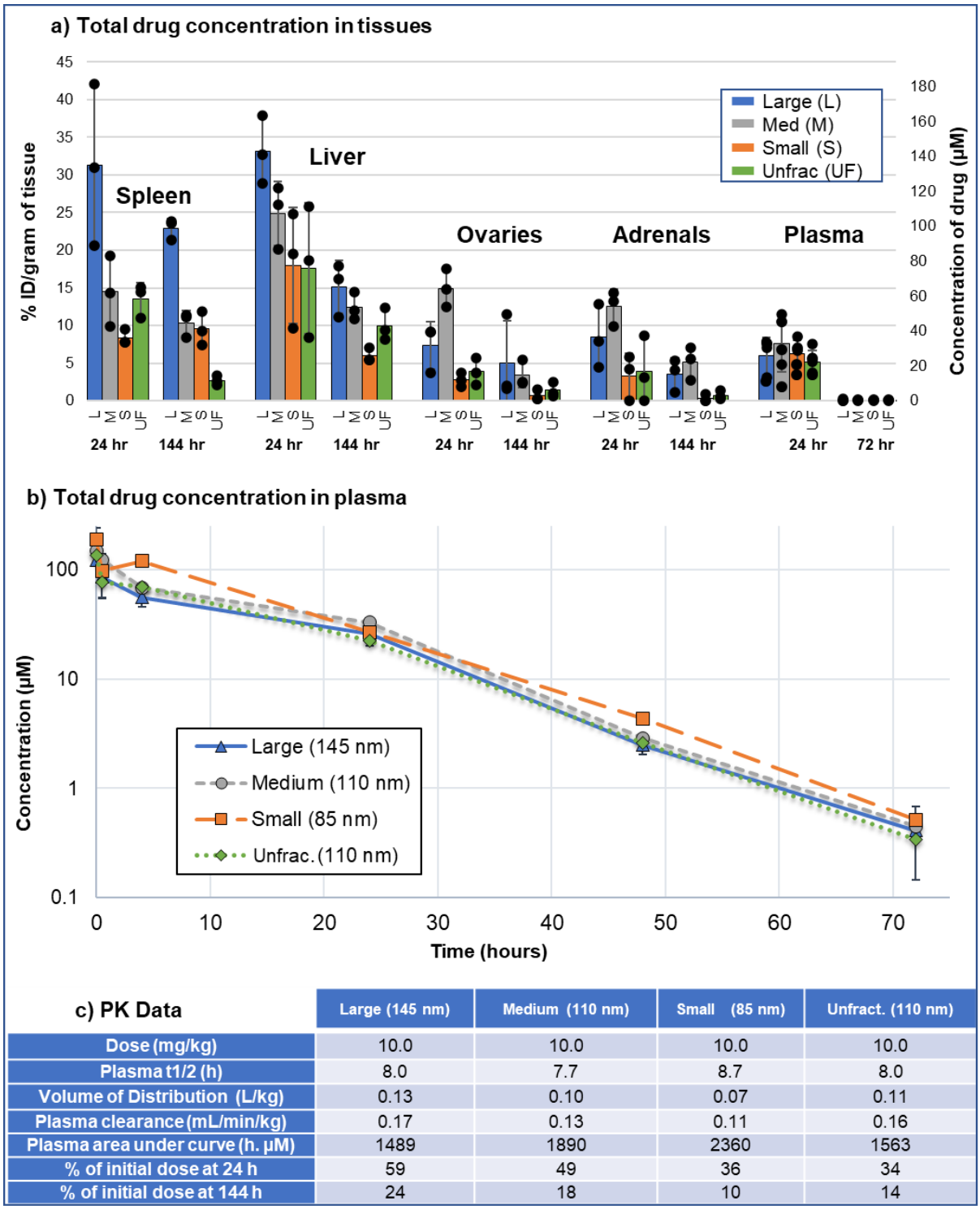

c) PK Data	Large (145 nm)	Medium (110 nm)	Small (85 nm)	Unfract. (110 nm)
Dose (mg/kg)	10.0	10.0	10.0	10.0
Plasma t1/2 (h)	8.0	7.7	8.7	8.0
Volume of Distribution (L/kg)	0.13	0.10	0.07	0.11
Plasma clearance (mL/min/kg)	0.17	0.13	0.11	0.16
Plasma area under curve (h. μM)	1489	1890	2360	1563
% of initial dose at 24 h	59	49	36	34
% of initial dose at 144 h	24	18	10	14

Figure 6. (a) Tissue drug concentrations, shown as concentration (right-hand axis) and initial dose per gram of tissue (%ID/g) (left-hand axis) for the 145 nm (large), 110 nm (medium), 85 nm (small) and unfractionated 110 nm AZDNPs. Individual data points are represented by black dots; the bar represents the average of all data points. Data at 24 and 144 hours is shown, except for plasma, which was 24 and 72 hours (final measured time point for plasma); (b) Corresponding plasma data; A zoomed-in section of the data and the numerical data for each time point are shown in Supplementary Information S.15; (c) PK parameters. Note that the percentage of the initial dose does not take muscle into account.

The percentage of the initial dose per gram of tissue (%ID/g) was measured at both 24 and 144 hours (**Figure 6a**). Shalgunov et al.[67] have previously reported on the %ID/g of NPs of ~ 100 nm size prepared using PLA/PEG with molecular weights of either 16,000 and 5000 in MX-1 tumor-bearing nude mice. In the present study it was found that spleen and liver concentrations were comparable to those of the 110 nm size fraction NPs, although the plasma %ID/g was considerably lower for the corresponding AZDNPs at (8 cf. ~20 %ID/g).[67] Bertrand et al.[21] determined

the effects of PEG density on liver uptake over a shorter time period of 6 hours and observed no size dependence when the PEG density was sufficiently high. In contrast, in the present study, there was clearly a correlation between NP size and liver uptake. However, in line with the present study, Bertrand et al.[21] did show a dependence upon NP size in respect to spleen uptake. The difference between our present study and the earlier studies by Bertrand et al.[21] and Shalgunov et al.[67] is the presence of the hydrophobic drug in the NPs and, in particular, its presence on the outer hydrated PEG shell (Supplementary Information S.2). One possibility is that the presence of the hydrophobic drug in the outer hydrated PEG shell results in the rapid uptake, by the reticuloendothelial system, of the NPs in which the drug is contained immediately after dosing. As a consequence, it would be expected that removal of drug from the outer hydrated PEG layer prior to administration of the NP would alter performance *in vivo*.

The plasma AUC and the spleen and liver concentrations for the 110 nm unfractionated AZDNPs were similar to those for the 110 nm size fraction AZDNPs, which implies that the significant proportion of low-drug-loaded NPs in the unfractionated formulation did not affect biodistribution. This finding suggests that the current study would not have benefitted from further optimization of the drug-polymer NP formulation by removing the low-drug-loaded NPs to increase the drug load. We have shown that the combined use of fractionation/separation and multi-technique analysis can enhance a proof-of-concept study in the early development phase, and can enable the widening of specifications or identify the paramount CQAs (the former, in this case).

To maximize plasma AUC using this drug-polymer system, one could focus on producing 85 nm size fraction AZDNPs. Smaller AZDNPs may further increase the plasma AUC, but at the detriment of drug loading would be significantly reduced (**Figure 2**). However, when comparing the 85 nm size fraction with the unfractionated batch, the plasma pharmacokinetic data were similar, so developing the 110 nm unfractionated formulation into a monodisperse 85 nm size formulation would not have led to a worthwhile improvement in the nanomedicine.

CONCLUSIONS

The current study allowed the correlation between the CQAs of fractionated hydrophobic drug-loaded PNPs (characterized using a range of advanced analytical techniques) and their biodistribution. Characterizing a polydisperse NP formulation is not a simple task. As demonstrated here, it is highly unlikely that conventional sizing techniques such as DLS, when used alone would ever be adequate for a full characterization of a formulation at the preclinical stage because of the lack of insight it generates into formulation properties. In contrast, we have demonstrated that NP fractionation/separation and subsequent analysis using a range of advanced characterization techniques such as SANS and SAXS, cryo-TEM and HAXPES, while currently not mainstream tools for the pharmaceutical development of nanomedicines, can uncover a wealth of insightful data, which helps understand NP behavior *in vivo*. In the present study, particularly noteworthy are size dependent observations including the accumulation in the adrenal glands and ovaries of 110 nm size fraction as well as the porous, hydrated nature of the NP core.

Significantly the present study has shown a general trend for the block co-polymer-drug NP system under study in terms of drug loading and rate of release, and the effect of increasing PEG packing density with particle size. The smaller the size of the NPs, the higher the NP dose (in terms of number), the higher the plasma AUC and the lower the uptake of drug, and presumably NP, by the RES. Importantly, however, further attempts at controlling the plasma AUC of this drug-polymer system by removal of low drug loading NPs would not have yielded significant improvements, and dosing the various size fractions *in vivo* gave an indication of how the variation in NP size and drug release rate affected the biodistribution, and negated the need to develop further formulations.

It is clear that the fractionation/separation of NP combined with multi-technique analysis enables a more detailed and data-rich faster assessment of nanomedicine performance when compared to conventional methodologies. Significantly, this combined approach is applicable to a range of NP types, as supported by a very recent study examining lipid NPs, which highlighted the presence of a large percentage of empty NPs in their formulation[68]. More studies such as this may identify further nuances in NP formulations and will aid in the widening of specifications for the clinical development of nanomedicines. Identification of CQAs, such as those described here, as early as possible during the development process can defined CQA ranges that ensure safety and efficacy *in vivo*. Such an endeavor is essential to guarantee consistent nanomedicine quality and clinical effectiveness.

METHODS

Nanoparticle Manufacture

Two batches of AZDNPs were manufactured by using an oil-in-water single-emulsion and solvent evaporation method at two different scales. The manufacturing process involved the preparation of an organic and an aqueous phase. The organic phase was prepared by dissolving 7% w/w of PLA-PEG 16/5 (DL-50:50) (Evonik, London, UK) and 3% w/w AZD5991 in 90% w/w dichloromethane (Sigma, Coventry, UK). For further details of AZD5991 drug substance synthesis, see reference[35]. The aqueous phase was prepared by making a 0.1% w/w sodium dodecyl sulfate solution (Sigma, Coventry, UK). Coarse emulsions were prepared by mixing both phases (ratio of 1:5) and homogenizing for 1 minute at 11,000 rpm, using an Ultra-Turrax T25 homogenizer (IKA, Stauffen, Germany). Immediately afterward, the resultant coarse emulsions were processed by using either an M-110F (for ~6.4 g scale) or an LM20 microfluidizer (for ~3 g scale) processor (Microfluidics, Newton, MA, USA). The coarse emulsion was passed through the processor once at 9000 psi (620 bar). The M-110F was equipped with two interaction chambers in series (F20Y 75 μm ceramic and H30Z 200 μm ceramic; Microfluidics), whereas the LM20 contained a single Y-type chamber (Diamond 75 μm F12Y; Microfluidics). Both microfluidizer processors had a cooling

coil immersed in an ice bath during processing. The resulting fine emulsions were then transferred to a rotatory evaporator (Bosch, Gerlingen, Germany) on an ice bath for 20 minutes to remove dichloromethane and to form the required NP suspensions. The suspensions were then diluted at a ratio of 1:5 in 20% cyclodextrin (200 mM HEPES [*N*-2-hydroxyethylpiperazine-*N*′-2-ethanesulfonic acid]) while being stirred on ice. After approximately 5 min, the diluted suspensions were transferred to a Tangential Flow Filtration system (Pall, Port Washington, NY, USA) to purify and further concentrate the NP suspensions while the mixture was kept at 5°C in an ice bath. Formulations requiring further manipulation were stored at 2–8°C. Formulations for storage were cryoprotected with 30% w/v sucrose and stored at –20°C until use.

Fractionation of NPs

Based on the work of Robertson et al.,[19] the NPs were separated into discrete size fractions using a Coulter Optima Max ultracentrifuge equipped with a TLA-55 rotor (Beckman Coulter, Brea, CA, USA). A total of 1000 µL of NP suspension was added to each centrifuge tube, and the NPs were subjected to 45 minutes of centrifugation at 2000 × *g*. The supernatant was carefully withdrawn from the tube and added to a new tube, and the remaining pellet was kept on ice for further manipulation. Approximately 50 µL of supernatant was left with the pellet to avoid disturbing the pellet. Subsequent separations were performed at 5000, 10,000, 20,000, 40,000, 60,000, 80,000, and 120,000 × *g*. All pellets were resuspended in approximately 200 µL of filtered deionized water and recombined where multiple sample replicates had been taken through the process. Fractions were either stored in a refrigerator (2–8°C) or cryoprotected with 30% w/w sucrose and stored at –20 °C. All NP sizes are expressed in terms of their diameter, and the fractions are referred to as the DLS-determined mean size. NPs appeared to be intact after fractionation based on the cryo-TEM images of NPs before and after fractionation.

Preparation of Pharmacokinetic Samples

Four samples were prepared for pharmacokinetic studies from the LM20 batch of AZDNPs, including the unfractionated batch. The 145-nm AZDNPs were prepared by combining the two fractions separated at 2000 × *g* and 5000 × *g*. (Fractions were combined because there was insufficient sample for the PK study.) For the 110 and 85 nm AZDNPs, the AZDNPs fractionated at 20,000 × *g* and 60,000 × *g* were used. Samples were subsequently filtered through a 0.45-µm filter for sterility (of a single-dose formulation). All samples were diluted to 2.0 mg/mL (drug concentration) by using a saturated sucrose solution filtered through a 0.45-µm filter to a final concentration of 30% w/w sucrose in phosphate-buffered saline (PBS) and stored at – 20°C. All NP sizes are expressed in terms of their diameter, and the PK samples are referred to as the DLS-determined mean size.

Drug Assay of Fractions and Unencapsulated Drug by HPLC-UV

A total of 50 µL of each AZDNP size fraction was added to 4.95 mL of 20% 2-hydroxypropyl-β-cyclodextrin (HP-β-CD) in 20 mM HEPES buffer (pH 7.4), vortexed, and stored at ambient temperature for 1 hour. A 500-µL aliquot was diluted with 500 µL of MeCN:H_2O (1:1) and analyzed for total drug concentration. The remaining mixture (1 mL) was ultracentrifuged at 186,000 × *g* at 4°C for 45 minutes, and 500 µL of supernatant was diluted with 500 µL of MeCN:H_2O (1:1) and analyzed for unencapsulated drug concentration with reversed-phase high-performance liquid chromatography with ultraviolet detection (HPLC-UV) (Supplementary Information S.16). A ± 5% error was estimated for the method.

***In Vitro* Release Test**

All release experiments were carried out under sink conditions, using sufficient drug to give a final concentration of 10 µg/mL drug in the dissolution medium of 20% w/v HP-β-CD (required to ensure drug solubility) in 20 mM HEPES buffer at pH 7.4. A total of 100 µL of each sample for release testing was diluted with 900 µL of dissolution media and vortexed before an aliquot (200–500 µL, depending on sample concentration) was diluted to 30 mL with preheated (37.1°C) release medium overnight and agitated at 75 rpm on a Thermo Shaker (Starlab, Brussels, Belgium) at 37.1°C in a water bath. Aliquots of 1 mL were collected at timed intervals and cooled on ice. Sampling was carried out at 0, 1, 2, 4, 6, 24, 30, 48, 54, 72, 144, 192, 240, 312, 409, 480, and 576 hours unless sufficient data beyond the NP half-life had been obtained. A 200-µL aliquot was collected for the determination of total concentration and diluted with 800 µL of H_2O:MeCN (1:1). Released drug was determined directly from the supernatant of the cooled solution after ultracentrifugation at 186,000 × *g* at 4°C for 45 minutes. Samples were analyzed by HPLC-UV (Supplementary Information S.16). Unencapsulated drug was removed from the release curve data by subtracting it from all released-drug data and then normalizing the data to encapsulated drug. $t_{50\%}$s were calculated for the first 200 hours of the release experiment. After this point, evaporation of the dissolution medium becomes significant and impacts the release curve. The release curve is composed of a quick and slow phase; to fit the drug release data, a two-phase association was performed by using Prism version 9.0.0 for Windows (GraphPad Software, San Diego, CA, USA). The first exponential for the quick phase was considered as the burst release, as described in the Results and Discussion section. The experiment was terminated when the AZDNP had released at least 50% of the drug content. Errors were calculated by using Prism, based on 95% confidence levels.

Gravimetric Drug Load

Samples of AZDNP (80 µL) were added to 20% HP-β-CD in 20 mM HEPES at pH 7.4 (920 µL) in pre-weighed vials and ultracentrifuged at 186,000 × *g* at 4°C. Supernatant was then removed from the diluted samples before the pellet was snap-frozen and the resulting sediment was freeze-dried. The resulting lyophile was weighed in triplicate. Drug loading (% w/w drug:total solids) was determined by using the determined amount of drug (mass concentration × formulation volume used) divided by the pellet mass. Samples were analyzed in duplicate, and an average was calculated. A ±5% error was estimated for the method.

NMR

AZDNP samples were diluted ×20 with deuterated acetone and sufficiently agitated to ensure that the drug and polymer were completely dissolved. Samples were transferred

to a 5-mm NMR tube. An internal standard was not used because only the ratio between the polymer and the drug weights was calculated. Analysis was carried out on an NEO 500 NMR instrument equipped with a TCI CryoProbe (Bruker, Billerica, MA, USA). Quantitative ^{1}H NMR data were acquired in duplicate, and an average value was taken. NMR parameters are outlined in Supplementary Information S.17. Data acquired with water suppression (using zgpr or noesypr1d pulse sequences) yielded values that were almost identical to those obtained with the analysis carried out without water suppression. The data reported do not include water suppression. All NMR spectra were acquired and interpreted with TopSpin software (version 4.0.0; Bruker) and Mnova NMR Chemist software (version 9.0.0-12821; Mestrelab, Hereford, UK). Manual-phase correction and automatic baseline correction was applied to each NMR spectrum. Manual integration was then conducted on three separate signals of the drug molecule, averaged, and compared against the two PLA multiplets at 1.43 and 5.08 ppm. The broad PEG signal (3.59 ppm) was not integrated due to the proximity of the dominant water signal (3.30 ppm), which interfered with the integration. The ratio was calculated in terms of a percentage of the total weight of drug to the total weight of polymer and drug, without considering the water content of the NPs or any other residual impurities of the formulation process. A ± 2% error was estimated for the method.

Dynamic Light Scattering and Zeta Potential

For size measurements, 20 µL of AZDNP was diluted to 1000 µL with 0.22-µm filtered water in disposable 1.5-mL plastic cuvettes. All DLS measurements were performed on a Zetasizer Nano ZS (Malvern Panalytical, Malvern, UK) at 25°C. Approximately 14–16 scans were completed for each DLS measurement and conducted in triplicate, using DTS software (version 5.10; Malvern), and the average was calculated. The standard deviation of the three measurements was used to determine the error. Zeta potential measurements were carried out in 700 µL of folded cells at 25°C. The applied voltage for an optimal electrophoretic mobility was determined by using the Malvern software auto function with phase analysis light scattering (PALS) and M3-PALS multi-frequency.[69]

Cryo-TEM

Samples were prepared at polymer and drug concentrations of approximately 2 mg/mL and dialyzed into PBS, pH 7.4, for 3 days at 4°C with several changes of the dialyzing bath solution. The grid used to hold the sample was a Quantifoil holey carbon R 1.2/1.3 300 mesh Cu (Agar Scientific, Stansted, UK). The grids were first discharged with a Pelco easiGlow system (Ted Pella, Redding, CA, USA) at 0.25 mBar for 1 minute before blotting with 2 µL of sample. The sample was quickly blotted and the grid and sample placed in liquid ethane to flash-freeze the sample and crystallization of water. Images were collected with a Titan Krios G2 electron microscope at 300 kV (Thermo Fisher Scientific, Waltham, MA, USA) equipped with a Falcon 2 direct electron detector (Thermo Fisher) at a nominal magnification of ×75,000 (1 Å/pixel), using EPU software (Thermo Fisher) with an electron fluence of ~50 Å^{-2}.

SANS and SAXS

Samples of AZDNP were measured for SANS on the Sans2d beamline at the ISIS Neutron and Muon Source (Rutherford Appleton Laboratory, Didcot, UK). AZDNPs were prepared at a concentration of 5 mg/mL (polymer and drug concentration) and dialyzed against 100% D_2O PBS over 24 hours, with five changes of dialyzing solution over 3 days. PBS was prepared by dissolving PBS powder (PBS, pH 7.4, P3813; Sigma Aldrich) in D_2O. For the 97-nm fractionated NPs (40,000 × g fraction), scattering was determined by measuring a number of D_2O/H_2O contrasts, as shown in **Table 3**.

Table 3. Series of D_2O/H_2O contrasts

D_2O/H_2O contrasts	D_2O/H_2O ratio (%)	Neutron SLD (10^{-6} Å^{-2})
Contrast 1	100	6.39
Contrast 2	56	3.33
Contrast 3	34	1.80
Contrast 4	0	–0.56

Samples of AZDNP were placed in clean, quartz circular cells of 1- or 2-mm path lengths (depending on the D_2O volume fraction[70]), and their SANS was measured at 25 ± 0.1°C. The SANS intensity, I(Q), of the sample was measured as a function of the scattering vector, $Q = (4\pi/\lambda)\sin(\theta/2)$, where θ is the scattering angle. The Q range explored was 0.0015-0.5 Å^{-1} through a white beam of 1.75–12.5 Å and two detectors positioned at 5 and 12 m from the sample. The I(Q) of the sample was obtained by subtracting the scattering from the solvent from the total measured intensity after the correction of both the sample and the solvent for transmission and detector efficiencies. Scattering was measured on an absolute scale by using the scattering from a standard sample (comprising a solid blend of protiated and perdeuterated polystyrene) in accordance with established procedures.

Small-angle X-ray scattering (SAXS) was used as a fifth "contrast." In X-ray scattering, deuterium and hydrogen have the same SLD. SAXS measurements were performed on a NanoinXider instrument (Xenocs, Sassenage, France) with a micro-focus sealed-tube, Cu 30 W/30 µm X-ray source (Cu K-α, λ = 1.54 Å). The scattered X-rays were detected on a Pilatus 3 hybrid photon counting detector (Dectris, Baden, Switzerland) at a distance of 938 mm from the sample stage. In this configuration, the X-ray instrument covered a Q range of 0.003–0.360 Å^{-1}. Samples were placed in 1-mm glass capillary tubes and measured at room temperature. Data reduction (azimuthal averaging, buffer subtraction, absolute scaling) was carried out using the Foxtrot software.

The geometrical models that were tested to fit the scattering data are described in the Results and Discussion section. For all models and the Guinier approximation, data analysis including least-squares refinements were performed by using SasView software.[71] The best fits to the SANS data were assessed first by the value of chi^2 obtained [71] whilst ensuring that the parameters to obtain this fit are within physical reasonable ranges. Note that the value of the chi^2 obtained

depends upon the number of parameters used in the fit. For a good fit chi^2 tends to 1.

Hard XPS

XPS analyses were carried out on an AXIS Supra spectrometer (Kratos Analytical, Manchester, UK), using monochromatic Al Kα and Ag Lα photon energies (20 mA, 15 kV). The instrument work function was calibrated to give a binding energy of 83.96 eV for the Au $4f_{7/2}$ line for metallic gold, and the spectrometer dispersion was adjusted to give a binding energy of 932.62 eV for the Cu $2p_{3/2}$ line of metallic copper. Survey scan analyses were carried out with an analysis area of 300 × 700 μm and a pass energy of 160 eV. High-resolution analyses were carried out with an analysis area of 300 × 700 μm and a pass energy of 40–80 eV. The instrument's energy-dependent intensity scale was calibrated by using methods for Ag Lα source calibration that were developed on this same instrument, and average-matrix relative sensitivity factors were used to account for the innate variation in intensity between different photoelectron peaks.[72]

Pharmacokinetic Study

Animals

All animal studies were conducted in accordance with UK Home Office legislation, the Animal Scientific Procedures Act of 1986, and the AstraZeneca Global Bioethics policy. All experimental work is outlined in project license P0EC1FFDF, which has gone through the AstraZeneca ethical review process. Athymic female nude mice were purchased from Envigo (Indianapolis, IN, USA). All mice weighed more than 18 g at the time of the first procedure.

Biodistribution of AZDNP

To determine the plasma and organ concentrations of the different diameter AZDNPs, naïve female nude mice (n = 6 per size) were injected intravenously with a single dose of small (85 nm), medium (110 nm), large (145 nm), or unfractionated (110 nm) AZDNP at a drug concentration of 10 mg/kg. Live bleeds were performed at various time points after doses were administered for determination of plasma levels of drug. Briefly, 20 μL of blood was collected from the tail vein with capillary tubes. Blood was diluted with 80 μL of PBS and centrifuged at 1917 × g for 5 minutes at 4°C. The supernatant was collected and stored at −80°C until analysis. Mice were killed via a Schedule 1 method, followed by secondary confirmation of death. Organs were collected at two time points (24 and 144 hours after dosing; n = 3 per size per time point) to compare the drug concentrations in liver, spleen, adrenal glands, ovaries, and thigh muscle. Tissues were rinsed with PBS, snap-frozen in liquid nitrogen, and stored at −80°C until analysis.

Plasma Bioanalysis

Each plasma sample (25 μL) was prepared by using an appropriate dilution factor and compared against an 11-point drug standard calibration curve (1–10,000 nM) prepared in dimethylsulfoxide and spiked into blank plasma. Acetonitrile (Fisher) (100 μL) was added with the internal standard, followed by centrifugation at 3000 rpm for 10 minutes. Supernatant (50 μL) was then diluted in 300 μL of water and analyzed by ultrahigh-performance liquid chromatography–tandem mass spectrometry (Supplementary Information S.18).

Tissue Bioanalysis

All tissues were weighed into fast preparation tubes containing Lysing Matrix A (MP Biomedicals, Leicestershire, UK). Water was added at an appropriate dilution ratio as a base for homogenization (2–10 times w/v). Homogenization was carried out in FastPrep-24 5G (MP Biomedicals, Santa Ana, CA, USA) at 6 m/s for 30 seconds. Each homogenate sample (25 μL) was compared against an 11-point drug standard calibration curve (1–10,000 nM) prepared in dimethylsulfoxide and spiked into blank tissue homogenate. Samples were then treated as plasma.

Percentage of Initial Dose

Total drug in the organ was determined as %ID/g, as calculated by Shalgunov et al.[67]:

$$\%\ \mathrm{ID/g} = \frac{[\text{concentration in tissue } (\mu g/g)]}{[\text{injected dose } (mg/kg)] \times [\text{animal weight } (g)]}$$

The percentage of the total initial dose was also calculated. For the weight of the organs, we used the measured values (spleen, 0.1584 g; liver, 1.330 g; adrenals, 0.0086 g; ovaries, 0.0240 g) with an estimate of the blood volume as 72 mL/kg[73] (average mouse, ∼29 g). All organs and plasma were assumed to have a density of 1.00 g/mL. The total weight of drug in each compartment was determined by multiplying the concentration by the organ weight.

Power Curves

Power curves were calculated in R (version 4.0.5), using the pwr.t.test function in the package pwr (version 1.3-0).[74] A one-tailed test, for which the effect size and standard deviation were required, was used. First, we considered the effect size. A fraction of the drug molecules are in solution as unencapsulated drug, and the remainder is present in the nanoparticles. Because only the drug present in the nanoparticles can contribute to burst events, the effect size of interest is assumed to be the burst fraction (burst) multiplied by 1 minus the unencapsulated drug fraction. Hence, control samples have unencapsulated drug levels equal to the unencapsulated drug, whereas burst samples have an unencapsulated drug level + burst (1 − unencapsulated drug). Standard deviations in each group were calculated by multiplying these expected means by the RSD. Subsequently, a pooled standard deviation was calculated (the square root of the sum of the variances), and the effect size was divided by the pooled standard deviation to obtain Cohen's D. Calculating the power at different burst fractions leads to the plots where fractions are expressed as percentages.

ASSOCIATED CONTENT

Supporting Information

S.1: A batch-to-batch comparison of AZDNP prepared on the M-110F and LM20. Data includes particle size, drug-drug polymer ratio, in vitro half-life of fractionated AZDNP
S.2: In vitro release analysis and burst release analysis of fractionated AZDNP
S.3: SANS scattering curve of unfractionated AZDNP
S.4: Cryo-transmission electron microscopy data of AZDNPs
S.5: SASview models used to fit the scattering data of AZDNP
S.6: Guinier approximation analysis of AZDNP

S.7: Scattering length densities of the difference components of AZDNP
S.8: Dimensions of the sub-structures contained in the fractionated AZDNP measured by SANS
S.9: Estimation of the PEG Density of the AZDNP fractions
S.10: Demonstration of a linear relationship AZDNP size and the R_g/R_H ratio
S.11: Hard XPS data and analysis
S.12: SANS core-shell model fitting for small AZDNP fractions
S.13: Cryo-Transmission Electron Micrographs of Unfractionated AZDNP
S.14: PK modeling and bioanalysis statistics
S.15: AZDNP Plasma PK Profiles: numerical data and a zoomed-in profile
S.16: Reverse-phase UPLC-UV method conditions for in vitro release analysis
S.17: NMR parameters for measuring DDPR
S.18: Bioanalysis UPLC method conditions

AUTHOR INFORMATION

Corresponding Authors

* Corresponding authors: Mark Jackman and Mariarosa Mazza, AstraZeneca, Granta Park, Great Abington, Cambridge CB21 6GH, UK; mark.jackman1@astrazeneca.com and mariarosa.mazza@astrazeneca.com.

Present Addresses

†Saif Baquain: Melville Laboratory for Polymer Synthesis, Yusuf Hamied Department of Chemistry, University of Cambridge, Cambridge, UK

‡Christine Madla: UCL School of Pharmacy, 29 – 39 Brunswick Square, London, WC1N 1AX

Author Contributions

Z.N., F.A., M.M, synthesized the AZDNPs. W.L. and M.J.J. planned and carried out the AZNP fractionation and the DLS analysis. M.J.L., W.L., M.J.J., K.T. planned the SANS experiments and obtained the beam time. M.J.L., W.L., M.J.J. and N.M., performed the experiments, and M.J.L., W.L., M.J.J., K.T. and N.M. analysed and interpreted the data. E.L., C.M., S.v.P., M.J.J. planned and carried out the NMR experiments. M.J.J. and S.S. planned the cryo-TEM imaging and C.M. analyzed data. A.S. carried out the bioanalysis. M.J.J., A.S., M.J.L., D.F., J.C. (AstraZeneca) carried out the bioanalytical validation analysis. A.S., J.M., M.M., M.J.J., A.P. planned the PK studies. J.M. and A.P. carried out the PK studies. D.W. and S.B. planned and carried out the in vitro release experiments. D.C, J.C. (Kratos), M.J.J., planned and carried out the HAXPES experiments, and D.C. analyzed the data. All authors contributed to the writing of the manuscript, approved the final version, and agree to be accountable for all aspects of the work.

Notes

This study was funded by AstraZeneca.
M.J.J., W.L., A.S., D.W, K.T., A.C., F.A., S.S., Z.N., J.C. (AstraZeneca), D.F., E.L., S.v.P., J.M., A.P., S.P., M.A., and M.M. are employees of AstraZeneca and hold stock ownership or stock interests in the company.
J.C. (Kratos) is an employee of Kratos (Shimadzu Group).
Experiments at the ISIS Neutron and Muon Source were supported by SANS beamtime allocation RB 1910321 (Correlating the Internal Structure of Drug-Loaded Polymeric Nanoparticles to Drug Release, DOI: 10.5286/ISIS.E.RB1910321) and the use of Nano-inXider SAXS system in the Materials Characterisation Laboratory.
This work benefited from the use of the SasView application, originally developed under National Science Foundation award DMR-0520547. SasView contains code developed with funding from the European Union's Horizon 2020 research and innovation program under the SINE2020 project, grant agreement no. 654000.
The work was also supported by the North West Centre of Advanced Drug Delivery (NoWCADD), a collaborative partnership between the Division of Pharmacy and Optometry, University of Manchester and AstraZeneca (http://www.nowcadd.manchester.ac.uk).

ACKNOWLEDGMENTS

The authors thank Pablo Hartmann, Pu Qian, and Kasim Sader from the Cambridge Pharmaceutical Cryo-EM Consortium for taking the beautiful cryo-TEM images and Laura Jarvis for technical expertise and data collection.

N.P.L. thanks funding by the UK Department of Business, Energy and Industrial Strategy through the National Measurement System programme.

The authors thank the Engineering and Physical Sciences Research Council for provision of a studentship on the Centre for Doctoral Training in Advanced Therapeutics and Nanomedicine (EP/L01646X) to Christine M. Madla.

The authors thank the Science and Technology Facilities Council for the provision of beamtime at the ISIS Neutron and Muon source.

REFERENCES

1. Leroux, J. C., Editorial: Drug Delivery: Too Much Complexity, Not Enough Reproducibility? *Angew. Chem. Int. Ed. Engl.* **2017,** *56*, 15170-15171.
2. Anselmo, A. C.; Mitragotri, S., Nanoparticles in the Clinic: An Update Post-COVID-19 Vaccines. *Bioeng. Transl. Med.* **2021,** *6* (3), e10246.
3. Ashford, M., Drug delivery—the increasing momentum. *Drug Delivery and Translational Research* **2020,** *10*, 1888-1894.
4. Martins, J. P.; das Neves, J.; de la Fuente, M.; Celia, C.; Florindo, H.; Günday-Türeli, N.; Popat, A.; Santos, J. L.; Sousa, F.; Schmid, R.; Wolfram, J.; Sarmento, B.; Santos, H. A., The Solid Progress of Nanomedicine. *Drug Deliv. Transl. Res.* **2020,** *10*, 726–729.
5. Lee, H.; Shields, A. F.; Siegel, B. A.; Miller, K. D.; Krop, I.; Ma, C. X.; LoRusso, P. M.; Munster, P. N.; Campbell, K.; Gaddy, D. F.; Leonard, S. C.; Geretti, E.; Blocker, S. J.; Kirpotin, D. B.; Moyo, V.; Wickham, T. J.; Hendriks, B. S., ^{64}Cu-MM-302 Positron Emission Tomography Quantifies Variability of Enhanced Permeability and Retention of Nanoparticles in Relation to Treatment Response in Patients with Metastatic Breast Cancer. *Clin. Cancer Res.* **2017,** *23* (15), 4190-4202.
6. Eliasof, S.; Lazarus, D.; Peters, C. G.; Case, R. I.; Cole, R. O.; Hwang, J.; Schluep, T.; Chao, J.; Lin, J.; Yen, Y.; Han, H.; Wiley, D. T.; Zuckerman, J. E.; Davis, M. E., Correlating preclinical animal studies and human clinical trials of a multifunctional, polymeric nanoparticle. *Proc. Natl. Acad. Sci. U. S. A.* **2013,** *110* (37), 15127-15132.
7. Troiano, G.; Nolan, J.; Parsons, D.; Van Geen Hoven, C.; Zale, S., A Quality by Design Approach to Developing and Manufacturing Polymeric Nanoparticle Drug Products. *AAPS J.* **2016,** *18*, 1354-1365.
8. Ashton, S.; Song, Y. H.; Nolan, J.; Cadogan, E.; Murray, J.; Odedra, R.; Foster, J.; Hall, P. A.; Low, S.; Taylor, P.; Ellston, R.; Polanska, U. M.; Wilson, J.; Howes, C.; Smith, A.; Goodwin, R. J. A.;

Swales, J. G.; Strittmatter, N.; Takáts, Z.; Nilsson, A.; Andren, P.; Trueman, D.; Walker, M.; Reimer, C. L.; Troiano, G.; Parsons, D.; De Witt, D.; Ashford, M.; Hrkach, J.; Zale, S.; Jewsbury, P. J.; Barry, S. T., Aurora Kinase Inhibitor Nanoparticles Target Tumors with Favorable Therapeutic Index In Vivo. *Sci. Transl. Med.* **2016,** *8* (325), 325ra17.

9. ClinicalTrials.gov Bioequivalence Study of IG-001 Versus Nab-Paclitaxel in Metastatic or Locally Recurrent Breast Cancer (TRIBECA). NCT 02064829. https://clinicaltrials.gov/ct2/show/NCT02064829.

10. ClinicalTrials.gov Efficacy Study of Genexol-PM and Cisplatin in Locally Advanced Head and Neck Cancer. NCT 01689194. https://clinicaltrials.gov/ct2/show/NCT01689194.

11. Birrenbach, G.; Speiser, P. P., Polymerized Micelles and Their Use as Adjuvants in Immunology. *J. Pharm. Sci.* **1976,** *65*, 1763-1766.

12. Dormont, F.; Rouquette, M.; Mahatsekake, C.; Gobeaux, F.; Peramo, A.; Brusini, R.; Calet, S.; Testard, F.; Lepetre-Mouelhi, S.; Desmaële, D.; Varna, M.; Couvreur, P., Translation of nanomedicines from lab to industrial scale synthesis: The case of squalene-adenosine nanoparticles. *Journal of Controlled Release* **2019,** *307*, 302-314.

13. Ashford, M. B.; England, R. M.; Akhtar, N., Highway to Success—Developing Advanced Polymer Therapeutics. *Adv. Ther.* **2021,** *4* (5), 2000285.

14. Maioli, V.; Chennell, G.; Sparks, H.; Lana, T.; Kumar, S.; Carling, D.; Sardini, A.; Dunsby, C., Time-lapse 3-D measurements of a glucose biosensor in multicellular spheroids by light sheet fluorescence microscopy in commercial 96-well plates. *Scientific Reports* **2016**.

15. Center for Drug Evaluation and Research, F., Drug Products, Including Biological Products, that Contain Nanomaterials - Guidance for Industry. **2022**.

16. Clogston, J. D.; Hackley, V. A.; Prina-Mello, A.; Puri, S.; Sonzini, S.; Soo, P. L., Sizing up the Next Generation of Nanomedicines. *Pharm. Res.* **2019,** *37*, 6.

17. Danaei, M.; Dehghankhold, M.; Ataei, S.; Hasanzadeh Davarani, F.; Javanmard, R.; Dokhani, A.; Khorasani, S.; Mozafari, M. R., Impact of Particle Size and Polydispersity Index on the Clinical Applications of Lipidic Nanocarrier Systems. *Pharmaceutics* **2018,** *10*, 57.

18. Wren, S.; Minelli, C.; Pei, Y.; Akhtar, N., Evaluation of Particle Size Techniques to Support the Development of Manufacturing Scale Nanoparticles for Application in Pharmaceuticals. *Journal of Pharmaceutical Sciences* **2020,** *109*, 2284-2293.

19. Robertson, J. D.; Rizzello, L.; Avila-Olias, M.; Gaitzsch, J.; Contini, C.; Magoń, M. S.; Renshaw, S. A.; Battaglia, G., Purification of Nanoparticles by Size and Shape. *Sci. Rep.* **2016,** *6*, 27494.

20. Hirn, S.; Semmler-Behnke, M.; Schleh, C.; Wenk, A.; Lipka, J.; Schäffler, M.; Takenaka, S.; Möller, W.; Schmid, G.; Simon, U.; Kreyling, W. G., Particle Size-Dependent and Surface Charge-Dependent Biodistribution of Gold Nanoparticles after Intravenous Administration. *Eur. J. Pharm. Biopharm.* **2011,** *77*, 407-416.

21. Bertrand, N.; Grenier, P.; Mahmoudi, M.; Lima, E. M.; Appel, E. A.; Dormont, F.; Lim, J.-M.; Karnik, R.; Langer, R.; Farokhzad, O. C., Mechanistic Understanding of In Vivo Protein Corona Formation on Polymeric Nanoparticles and Impact on Pharmacokinetics. *Nat Commun* **2017,** *8*, 777.

22. Erdoğar, N.; Varan, G.; Varan, C.; Bilensoy, E., Biodistribution of Polymeric, Polysaccharide and Metallic Nanoparticles. In *Characterization of Pharmaceutical Nano and Microsystems*, Peltonen, L., Ed. John Wiley & Sons: Hoboken, NJ, 2021; pp 275-290.

23. He, C.; Hu, Y.; Yin, L.; Tang, C.; Yin, C., Effects of particle size and surface charge on cellular uptake and biodistribution of polymeric nanoparticles. *Biomaterials* **2010,** *31*, 3657-3666.

24. Caster, J. M.; Yu, S. K.; Patel, A. N.; Newman, N. J.; Lee, Z. J.; Warner, S. B.; Wagner, K. T.; Roche, K. C.; Tian, X.; Min, Y.; Wang, A. Z., Effect of Particle Size on the Biodistribution,Toxicity, and Efficacy of Drug-Loaded Polymeric Nanoparticles in Chemoradiotherapy. *Nanomed. Nanotechnol. Biol. Med.* **2017,** *13*, 1673-1683.

25. Suk, J. S.; Xu, Q.; Kim, N.; Hanes, J.; Ensign, L. M., PEGylation as a Strategy for Improving Nanoparticle-Based Drug and Gene Delivery. *Adv. Drug Deliv. Rev.* **2016,** *99*, 28-51.

26. Fam, S. Y.; Chee, C. F.; Yong, C. Y.; Ho, K. L.; Mariatulqabtiah, A. R.; Tan, W. S., Stealth Coating of Nanoparticles in Drug-Delivery Systems. *Nanomaterials* **2020,** *10* (4).

27. Owens, D. E.; Peppas, N. A., Opsonization, biodistribution, and pharmacokinetics of polymeric nanoparticles. *International Journal of Pharmaceutics* **2006,** *307* (1), 93-102.

28. Kaza, M.; Karaźniewicz-Łada, M.; Kosicka, K.; Siemiątkowska, A.; Rudzki, P. J., Bioanalytical method validation: new FDA guidance vs. EMA guideline. Better or worse? *Journal of Pharmaceutical and Biomedical Analysis* **2019,** *165*, 381-385.

29. Marini, J. C.; Anderson, M.; Cai, X. Y.; Chappell, J.; Coffey, T.; Gouty, D.; Kasinath, A.; Koppenburg, V.; Oldfield, P.; Rebarchak, S.; Bowsher, R. R., Systematic Verification of Bioanalytical Similarity Between a Biosimilar and a Reference Biotherapeutic: Committee Recommendations for the Development and Validation of a Single Ligand-Binding Assay to Support Pharmacokinetic Assessments. *Botanical Review* **2014,** *16*, 1149-1158.

30. Song, W.; Tweed, J. A.; Visswanathan, R.; Saunders, J. P.; Gu, Z.; Holliman, C. L., Bioanalysis of Targeted Nanoparticles in Monkey Plasma via LC-MS/MS. *Analytical Chemistry* **2019,** *91*, 13874-13882.

31. Stern, S. T.; Martinez, M. N.; Stevens, D. M., When Is It Important to Measure Unbound Drug in Evaluating Nanomedicine Pharmacokinetics? *Drug Metab. Dispos.* **2016,** *44*, 1934-1939.

32. Hrkach, J.; Von Hoff, D.; Ali, M. M.; Andrianova, E.; Auer, J.; Campbell, T.; De Witt, D.; Figa, M.; Figueiredo, M.; Horhota, A.; Low, S.; McDonnell, K.; Peeke, E.; Retnarajan, B.; Sabnis, A.; Schnipper, E.; Song, J. J.; Song, Y. H.; Summa, J.; Tompsett, D.; Troiano, G.; Van Geen Hoven, T.; Wright, J.; LoRusso, P.; Kantoff, P. W.; Bander, N. H.; Sweeney, C.; Farokhzad, O. C.; Langer, R.; Zale, S., Preclinical Development and Clinical Translation of a PSMA-Targeted Docetaxel Nanoparticle with a Differentiated Pharmacological Profile. *Sci. Transl. Med.* **2012,** *4*, 128ra39 LP - 128ra39.

33. Liu, T.; Xu, F.; Thieme, E.; Lam, V.; Fan, G.; Nikolaenko, L.; Kurtz, S. E.; Tyner, J. W.; Danilova, O.; Danilov, A., Pharmacologic Targeting MCL1 with AZD5991 Induces Apoptosis and Mitochondrial Dysfunction in Non-Hodgkin Lymphoma (NHL) Cells. *Blood* **2020,** *136*, 33.

34. Matulis, S. M.; Gupta, V. A.; Brown, I.; Keats, J. J.; Secrist, P.; Cidado, J.; Tron, A. E.; Neri, P.; Bahlis, N.; Kaufman, J. L.; Heffner, L.; Lonial, S.; Nooka, A. K.; Boise, L. H., Preclinical Activity of Novel MCL1 Inhibitor AZD5991 in Multiple Myeloma. *Blood* **2018,** *132*, 952.

35. Tron, A. E.; Belmonte, M. A.; Adam, A.; Aquila, B. M.; Boise, L. H.; Chiarparin, E.; Cidado, J.; Embrey, K. J.; Gangl, E.; Gibbons, F. D.; Gregory, G. P.; Hargreaves, D.; Hendricks, J. A.; Johannes, J. W.; Johnstone, R. W.; Kazmirski, S. L.; Kettle, J. G.; Lamb, M. L.; Matulis, S. M.; Nooka, A. K.; Packer, M. J.; Peng, B.; Rawlins, P. B.; Robbins, D. W.; Schuller, A. G.; Su, N.; Yang, W.; Ye, Q.; Zheng, X.; Secrist, J. P.; Clark, E. A.; Wilson, D. M.; Fawell, S. E.; Hird, A. W., Discovery of Mcl-1-specific inhibitor AZD5991 and preclinical activity in multiple myeloma and acute myeloid leukemia. *Nature Communications* **2018,** *9* (1), 5341.

36. Alliod, O.; Almouazen, E.; Nemer, G.; Fessi, H.; Charcosset, C., Comparison of Three Processes for Parenteral Nanoemulsion Production: Ultrasounds, Microfluidizer, and Premix Membrane Emulsification. *Journal of Pharmaceutical Sciences* **2019,** *108* (8), 2708-2717.

37. Mahdavi, Z.; Rezvani, H.; Keshavarz Moraveji, M., Core–shell nanoparticles used in drug delivery-microfluidics: a review. *RSC Advances* **2020,** *10* (31), 18280-18295.

38. Huang, W.; Tsui, C. P.; Tang, C. Y.; Gu, L., Effects of Compositional Tailoring on Drug Delivery Behaviours of Silica Xerogel/Polymer Core-shell Composite Nanoparticles. *Scientific Reports* **2018,** *8* (1), 13002.

39. Mares, A. G.; Pacassoni, G.; Marti, J. S.; Pujals, S.; Albertazzi, L., Formulation of tunable size PLGA-PEG nanoparticles for drug delivery using microfluidic technology. *PLOS ONE* **2021,** *16* (6), e0251821.

40. Rodrigues de Azevedo, C.; von Stosch, M.; Costa, M. S.; Ramos, A. M.; Cardoso, M. M.; Danhier, F.; Préat, V.; Oliveira, R., Modeling of the burst release from PLGA micro- and nanoparticles as function of physicochemical parameters and formulation characteristics. *International Journal of Pharmaceutics* **2017,** *532* (1), 229-240.

41. D'souza, A. A.; Shegokar, R., Polyethylene glycol (PEG): a versatile polymer for pharmaceutical applications. *Expert Opinion on Drug Delivery* **2016,** *13* (9), 1257-1275.

42. Heald, C. R.; Stolnik, S.; Kujawinski, K. S.; De Matteis, C.; Garnett, M. C.; Illum, L.; Davis, S. S.; Purkiss, S. C.; Barlow, R. J.; Gellert,

P. R., Poly(lactic acid)−Poly(ethylene oxide) (PLA−PEG) Nanoparticles: NMR Studies of the Central Solidlike PLA Core and the Liquid PEG Corona. *Langmuir* **2002,** *18* (9), 3669−3675.
43. Schindelin, J.; Arganda-Carreras, I.; Frise, E.; Kaynig, V.; Longair, M.; Pietzsch, T.; Preibisch, S.; Rueden, C.; Saalfeld, S.; Schmid, B.; Tinevez, J.-Y.; White, D. J.; Hartenstein, V.; Eliceiri, K.; Tomancak, P.; Cardona, A., Fiji: an open-source platform for biological-image analysis. *Nature Methods* **2012,** *9*, 676-682.
44. Rueden, C. T.; Schindelin, J.; Hiner, M. C.; DeZonia, B. E.; Walter, A. E.; Arena, E. T.; Eliceiri, K. W., ImageJ2: ImageJ for the Next Generation of Scientific Image Data. *BMC Bioinformatics* **2017,** *18*, 529.
45. Kline, S. R., Reduction and Analysis of SANS and USANS Data using IGOR Pro. *J. Appl. Crystallogr.* **2006,** *39*, 895-900.
46. Feigin, L. A.; Svergun, D. I., *Structure Analysis by Small-Angle X-Ray and Neutron Scattering*. Springer: Boston, MA, 1987.
47. Guinier, A.; Fournet, G., *Small-Angle Scattering of X-Rays*. John Wiley & Sons: Hoboken, NJ, 1955.
48. Science and Technology Facilities Council Sans2D: Time-of-Flight Small-Angle Neutron Scattering Instrument. https://www.isis.stfc.ac.uk/Pages/sans2d.aspx (accessed December 3, 2021).
49. Butler, P.; King, S. SASView Fitting. https://www.sasview.org/docs/user/qtgui/Perspectives/Fitting/fitting_help.html (accessed December 3, 2021).
50. Shi, L.; Zhang, J.; Zhao, M.; Tang, S.; Cheng, X.; Zhang, W.; Li, W.; Liu, X.; Peng, H.; Wang, Q., Effects of polyethylene glycol on the surface of nanoparticles for targeted drug delivery. *Nanoscale* **2021,** *13* (24), 10748-10764.
51. Kratochvíl, P.; Netopilík, M., The effect of nanoparticle nonuniformity on the ratio of gyration and hydrodynamic radiuses. *International Journal of Polymer Analysis and Characterization* **2017,** *22* (2), 112-117.
52. Belsey, N. A.; Shard, A. G.; Minelli, C., Analysis of protein coatings on gold nanoparticles by XPS and liquid-based particle sizing techniques. *Biointerphases* **2015,** *10* (1), 019012.
53. Minelli, C.; Shard, A. G., Chemical measurements of polyethylene glycol shells on gold nanoparticles in the presence of aggregation. *Biointerphases* **2016,** *11* (4), 04b306.
54. Shard, A. G., A Straightforward Method for Interpreting XPS Data from Core-Shell Nanoparticles. *J. Phys. Chem. C Nanomater. Interfaces* **2012,** *116*, 16806-16813.
55. Cant, D. J. H.; Wang, Y.-C.; Castner, D. G.; Shard, A. G., A Technique for Calculation of Shell Thicknesses for Core-Shell-Shell Nanoparticles from XPS Data. *Surf. Interface Anal.* **2016,** *48*, 274-282.
56. Kalbe, H.; Rades, S.; Unger, W. E. S., Determining Shell Thicknesses in Stabilised CdSe@ZnS Core-Shell Nanoparticles by Quantitative XPS Analysis using an Infinitesimal Columns Model. *J. Electron Spectrosc. Relat. Phenom.* **2016,** *212*, 34-43.
57. U.S. Food and Drug Administration, Bioanalytical Method Validation: Guidance for Industry. Center for Drug Evaluation and Research, Center for Veterinary Medicine: Rockville, MD, 2020.
58. Sørensen, K. K.; McCourt, P.; Berg, T.; Crossley, C.; Couteur, D. L.; Wake, K.; Smedsrød, B., The Scavenger Endothelial Cell: A New Player in Homeostasis and Immunity. *Am. J. Physiol. Regul. Integr. Comp. Physiol.* **2012,** *303* (12), R1217-R1230.
59. Park, J.-K.; Utsumi, T.; Seo, Y.-E.; Deng, Y.; Satoh, A.; Saltzman, W. M.; Iwakiri, Y., Cellular Distribution of Injected PLGA-Nanoparticles in the Liver. *Nanomed. Nanotechnol. Biol. Med.* **2016,** *12* (5), 1365-1374.
60. Lammers, T., Just dose it. *Nature Materials* **2020,** *19*, 1257-1258.
61. Ouyang, B.; Poon, W.; Zhang, Y. N.; Lin, Z. P.; Kingston, B. R.; Tavares, A. J.; Zhang, Y.; Chen, J.; Valic, M. S.; Syed, A. M.; MacMillan, P.; Couture-Senécal, J.; Zheng, G.; Chan, W. C. W., The Dose Threshold for Nanoparticle Tumour Delivery. *Nat. Mater.* **2020,** *19* (12), 1362-1371.
62. Poley, M.; Mora-Raimundo, P.; Shammai, Y.; Kaduri, M.; Koren, L.; Adir, O.; Shklover, J.; Shainsky-Roitman, J.; Ramishetti, S.; Man, F.; de Rosales, R. T. M.; Zinger, A.; Peer, D.; Ben-Aharon, I.; Schroeder, A., Nanoparticles Accumulate in the Female Reproductive System during Ovulation Affecting Cancer Treatment and Fertility. *ACS Nano* **2022**.
63. Weiss, V. M.; Lucas, H.; Mueller, T.; Chytil, P.; Etrych, T.; Naolou, T.; Kressler, J.; Mäder, K., Intended and Unintended Targeting of Polymeric Nanocarriers: The Case of Modified Poly(glycerol adipate) Nanoparticles. *Macromol Biosci* **2018,** *18*, 1700240.
64. Poley, M.; Chen, G.; Sharf-Pauker, N.; Avital, A.; Kaduri, M.; Sela, M.; Raimundo, P. M.; Koren, L.; Arber, S.; Egorov, E.; Shainsky, J.; Shklover, J.; Schroeder, A., Sex-Based Differences in the Biodistribution of Nanoparticles and Their Effect on Hormonal, Immune, and Metabolic Function. *Advanced NanoBiomed Research* **2022,** *n/a* (n/a), 2200089.
65. Schädlich, A.; Hoffmann, S.; Mueller, T.; Caysa, H.; Rose, C.; Göpferich, A.; Li, J.; Kuntsche, J.; Mäder, K., Accumulation of nanocarriers in the ovary: A neglected toxicity risk? *Journal of Controlled Release* **2012,** *160* (1), 105-112.
66. Patterson, C. M.; Balachander, S. B.; Grant, I.; Pop-Damkov, P.; Kelly, B.; McCoull, W.; Parker, J.; Giannis, M.; Hill, K. J.; Gibbons, F. D.; Hennessy, E. J.; Kemmitt, P.; Harmer, A. R.; Gales, S.; Purbrick, S.; Redmond, S.; Skinner, M.; Graham, L.; Secrist, J. P.; Schuller, A. G.; Wen, S.; Adam, A.; Reimer, C.; Cidado, J.; Wild, M.; Gangl, E.; Fawell, S. E.; Saeh, J.; Davies, B. R.; Owen, D. J.; Ashford, M. B., Design and optimisation of dendrimer-conjugated Bcl-2/xL inhibitor, AZD0466, with improved therapeutic index for cancer therapy. *Communications Biology* **2021,** *4* (1), 112.
67. Shalgunov, V.; Zaytseva-Zotova, D.; Zintchenko, A.; Levada, T.; Shilov, Y.; Andreyev, D.; Dzhumashev, D.; Metelkin, E.; Urusova, A.; Demin, O.; McDonnell, K.; Troiano, G.; Zale, S.; Safarova, E., Comprehensive study of the drug delivery properties of poly(l-lactide)-poly(ethylene glycol) nanoparticles in rats and tumor-bearing mice. *Journal of Controlled Release* **2017,** *261*, 31-42.
68. Li, S.; Hu, Y.; Li, A.; Lin, J.; Hsieh, K.; Schneiderman, Z.; Zhang, P.; Zhu, Y.; Qiu, C.; Kokkoli, E.; Wang, T.-H.; Mao, H.-Q., Payload distribution and capacity of mRNA lipid nanoparticles. *Nature Communications* **2022,** *13* (1), 5561.
69. Malvern Instruments, Zetasizer Nano Series. Worcestershire, UK.
70. Heenan, R. K.; Penfold, J.; King, S. M., SANS at Pulsed Neutron Sources: Present and Future Prospects. *Journal of Applied Crystallography* **2007,** *30*.
71. SASView website. http://www.sasview.org/.
72. Shard, A. G.; Counsell, J. D. P.; Cant, D. J. H.; Smith, E. F.; Navabpour, P.; Zhang, X.; Blomfield, C. J., Intensity Calibration and Sensitivity Factors for XPS Instruments with Monochromatic Ag Lα and Al Kα Sources. *Surf. Interface Anal.* **2019,** *51*, 763-773.
73. Diehl, K. H.; Hull, R.; Morton, D.; Pfister, R.; Rabemampianina, Y.; Smith, D.; Vidal, J. M.; van de Vorstenbosch, C., A Good Practice Guide to the Administration of Substances and Removal of Blood, Including Routes and Volumes. *J. Appl. Toxicol.* **2001,** *21* (1), 15-23.
74. Champely, S., pwr: Basic Functions for Power Analysis. R package version 1.3-0. **2020**.